Table 1. Genes associated with nucleic acid metabolism overexpressed in hepatocellular carcinoma

Tag sequence	Normal liver	Non-cancerous liver	HCC	Fold*	Gene	*P*-value†
CAGCTCCGCT	0	2	11	5.5	dUTP pyrophosphatase	0.010
AAAGGATAAT	0	0	3	> 3	General transcription factor II H, polypeptide 2	0.127
ACGGTCCAGG	0	0	3	> 3	Cytidine deaminase	0.127
ATGTAGAGTG	0	0	3	> 3	Thymidylate synthase	0.127
TGGGGATTAC	1	0	3	> 3	Zinc ribbon domain containing, 1	0.127
CACCCTGTAC	2	2	6	3	Solute carrier family 29	0.147
GAACGCCTAA	1	1	3	3	Dihydropyrimidinase-like 2	0.308
GCGCTGGTAC	0	1	3	3	2′-5′-oligoadenylate synthetase 3	0.308
CTTAGTGCAA	0	2	4	2	3′-phosphoadenosine 5′-phosphosulphate synthase 2	0.335
TTGTTACATC	0	2	3	1.5	Phosphoribosyl pyrophosphatase synthetase-associated protein 1	0.506

*Fold increase was calculated by dividing the number of tags in HCC by that of tags in non-cancerous liver. To avoid division by 0, a tag value of 1 was used for any tag that was not detectable in one sample.

†Statistical significance of differentially expressed genes between two groups (HCC and non-cancerous liver libraries) was calculated using Monte Carlo simulation.

HCC, hepatocellular carcinoma.

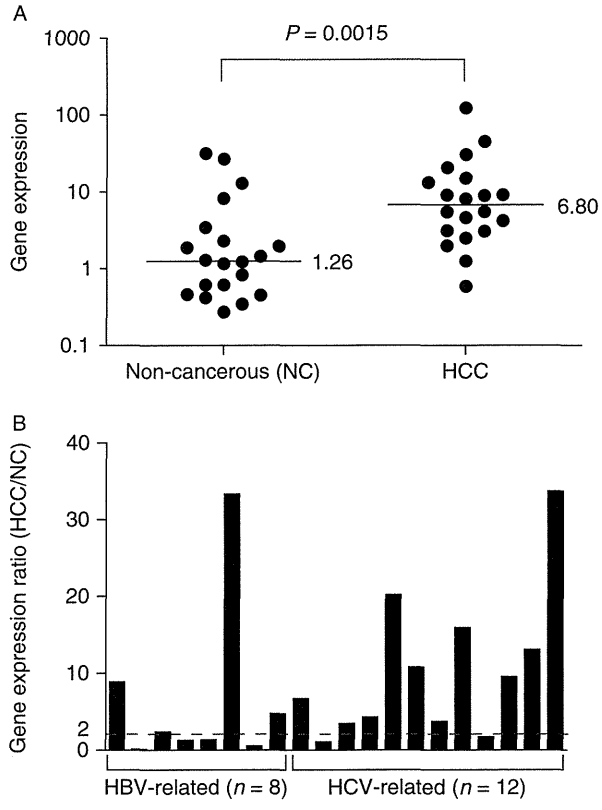

Fig. 1. (A) Quantitative reverse transcription-polymerase chain reaction analysis of *DUT* expression in hepatocellular carcinoma (HCC) and corresponding non-cancerous liver tissues. *DUT* was significantly activated in HCC tissues compared with non-cancerous liver tissues ($P = 0.0015$). A median value in each group is indicated. (B) *DUT* gene expression ratios of HCC and corresponding non-cancerous liver tissues. Fourteen of 20 HCC tissues expressed *DUT* more than two-fold compared with the background non-cancerous liver tissues. HBV, hepatitis B virus; HCV, hepatitis C virus.

Interestingly, *DUT* gene knockdown not only suppressed cell proliferation but also sensitized HuH7 cells to low-dose 5-FU (Fig. 2F and Fig. S3B). These data suggest that dUTPase overexpression in HCC tissues may be associated with enhanced cell proliferation and 5-FU resistance.

Intense dUTP pyrophosphatase expression is correlated with a poor prognosis in hepatocellular carcinoma patients

To characterize the clinicopathological characteristics of dUTPase expression in HCC, we performed IHC using an additional independent HCC cohort. Accordingly, we explored the dUTPase expression in HCC using 82 formalin-fixed paraffin-embedded HCC specimens. All HCC tissues were surgically resected at the Liver Disease Center of Kanazawa University Hospital with full clinical information, and their immunoreactivity to anti-dUTPase antibodies was evaluated by IHC. We noticed that anti-dUTPase antibodies reacted to both nuclear (red arrows) and cytoplasmic (blue arrows) isoforms of dUTPase, as described previously (26) (Fig. 3A and B). We therefore evaluated the nuclear and cytoplasmic expression of dUTPase separately. We stratified HCC tissues and evaluated the dUTPase expression status based on the percentages of dUTPase-positive cells. The frequency of nuclear or cytoplasmic dUTPase-positive cells was highly variable in each HCC tissue, and we defined HCCs with nuclear or cytoplasmic dUTPase expressed in $\geq 50\%$ of tumour cells as nuclear or cytoplasmic dUTPase-high HCC (Fig. 3C). Nuclear dUTPase overexpression was detected in 36.6% (30 of 82), whereas cytoplasmic dUTPase overexpression was detected in 67.1% (55 of 82) of HCC tissues compared with the corresponding non-cancerous liver tissues

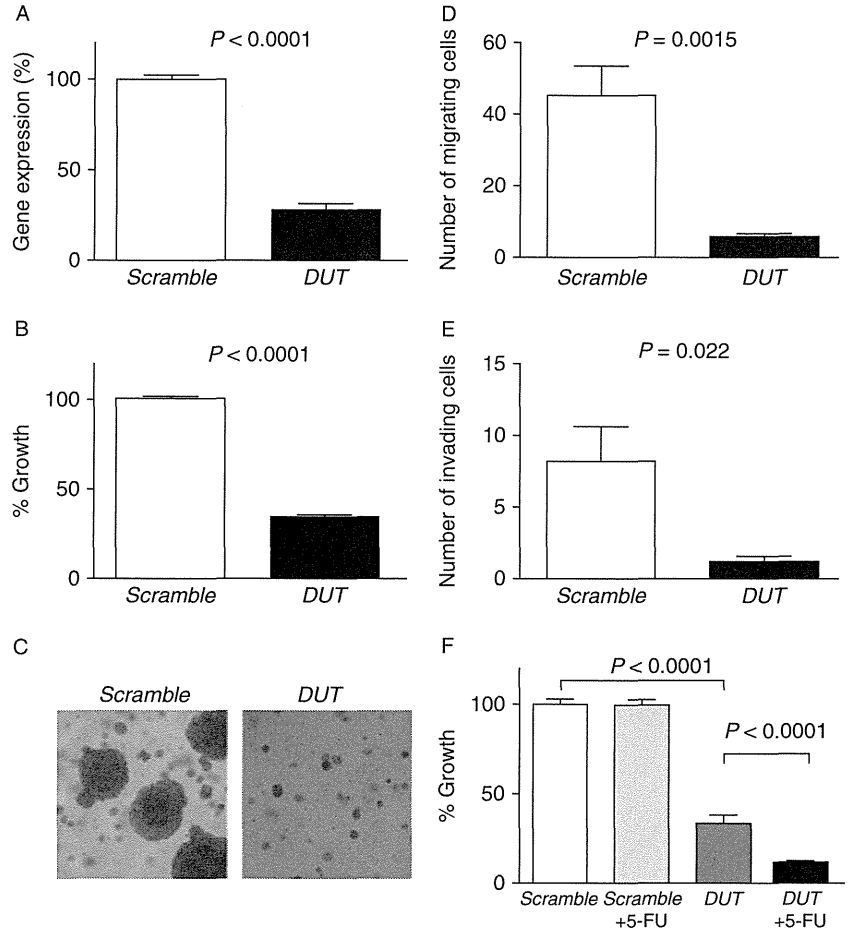

Fig. 2. (A) Transfection of small interfering RNAs targeting *DUT* (DUT1) decreased *DUT* expression compared with the control (scrambled sequence). Gene expression was evaluated in triplicate 72 h after transfection (mean ± SD). (B) *DUT* gene knockdown significantly suppressed cell proliferation ($P < 0.0001$). Cell viability was evaluated in triplicate 72 h after transfection (mean ± SD). (C) Soft agar assay. *DUT* gene knockdown suppressed anchorage-independent cell growth. (D and E) Matrigel invasion assay. *DUT* gene knockdown decreased the numbers of both migrating and invading cells. Experiments were performed in triplicate (mean ± SD). (F) *DUT* gene knockdown sensitized HuH7 cells to low-dose 5-fluorouracil (5-FU) (0.25 μg/ml), which had no effect on the cell proliferation in the control (mean ± SD).

(Table 2). In general, non-cancerous hepatocytes rarely expressed nuclear dUTPase (Fig. 3A).

We investigated the clinicopathological characteristics of nuclear or cytoplasmic dUTPase in low /high HCC cases (Table 2). The expression status of nuclear dUTPase showed no correlation with age, gender, virus, presence of cirrhosis, α-fetoprotein value, tumour size and TNM stages. However, nuclear dUTPase expression was significantly correlated with the histological grades of HCC ($P = 0.0099$), and high frequencies of nuclear dUTPase-positive cells were associated with poorly differentiated cell morphology in the HCC tissue. In contrast, cytoplasmic dUTPase expression was not correlated with the histological grades of HCC ($P = 0.077$). We examined the cell proliferation of these HCC samples by PCNA staining, and PCNA indexes were significantly higher in nuclear dUTPase high HCC than low HCC with statistical significance ($P = 0.01$) (Fig. S4).

We further investigated the prognostic significance of dUTPase expression in HCC. Strikingly, high nuclear dUTPase expression in HCC tissue correlated with a poor survival outcome compared with low nuclear dUTPase expression ($P = 0.0036$), whereas high cytoplasmic dUTPase expression had little effects when evaluated by recurrence-free survival (Fig. 3D). Furthermore, univariate Cox regression analysis showed a significant correlation between high nuclear dUTPase expression and a high risk of mortality (HR, 2.47; 95% CI, 1.08–5.66; $P = 0.032$; Table 3). By multivariate Cox regression analysis, TNM stage (HR, 2.75; 95% CI, 1.11–6.79; $P = 0.027$) and nuclear dUTPase (HR, 2.61; 95% CI, 1.13–6.05; $P = 0.024$) were independent prognostic factors associated with a high risk of mortality, and other clinicopathological features did not add independent prognostic information. These data indicate a significant correlation between the malignant potential of

Liver International (2009)

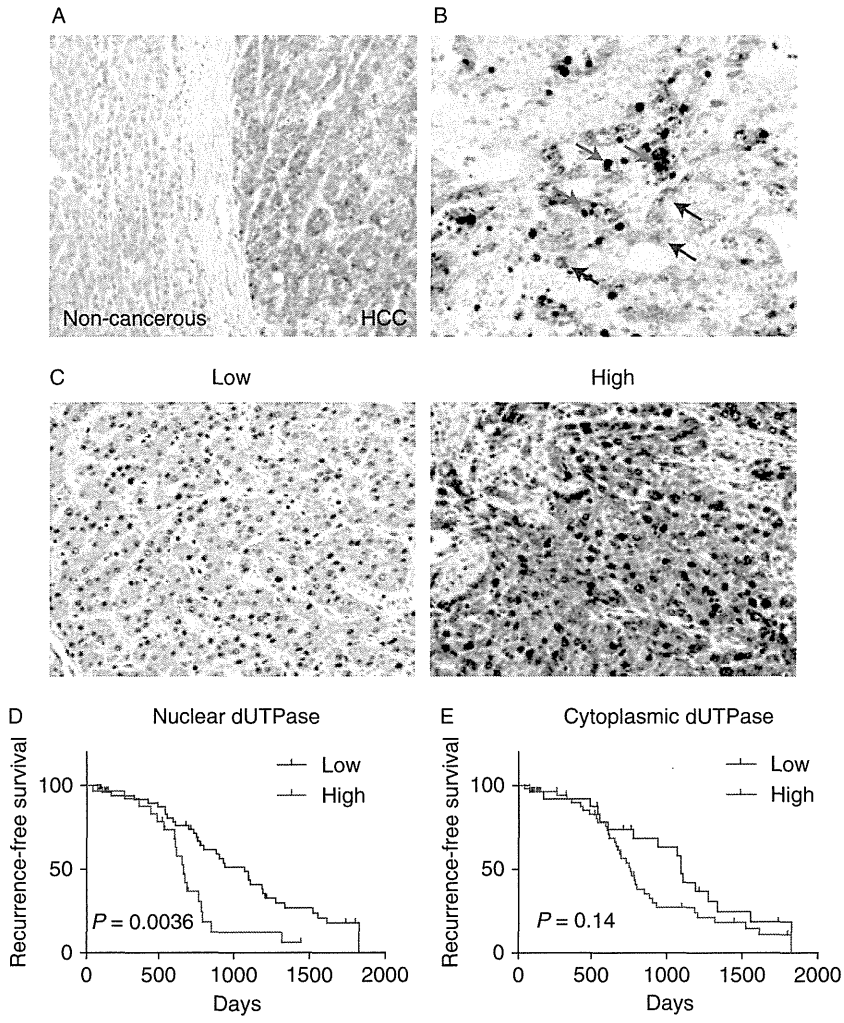

Fig. 3. Immunohistochemistry analysis of dUTP pyrophosphatase (dUTPase) expression in hepatocellular carcinoma (HCC). (A) A representative photomicrograph of dUTPase staining in an HCC and adjacent non-cancerous liver tissue. (B) A representative photomicrograph of dUTPase staining in an HCC. Both nuclear (red arrows) and cytoplasmic (blue arrows) forms of dUTPase were detected. (C) Representative photomicrographs of HCC tissues with low (0–50%) and high (≥50%) frequencies of nuclear and cytoplasmic dUTPase-positive cells. (D and E) Kaplan–Meier survival analysis of HCC tissues with nuclear (D) or cytoplasmic (E) dUTPase expression. High percentages of nuclear dUTPase-positive tumour cells significantly correlated with poor clinical outcome in recurrence-free survival.

HCC and nuclear dUTPase expression, implicating the potential effectiveness of nuclear dUTPase level as a biomarker for predicting the survival of HCC patients after surgical resection.

Discussion

Here, using a global gene expression profiling approach (18), we have identified the activation of the nucleotide/nucleoside metabolism-related gene *DUT* (encoding dUTPase) in HCC. Notably, an intense dUTPase expression was detected in a subset of HCC with a poor prognosis. To the best of our knowledge, this is the first report describing the correlation between dUTPase activation and poor survival outcome in HCC patients.

In normal cells, dUTPase is known to catalyse the hydrolysis of dUTP to dUMP in order to maintain the dUMP pool at a certain level for thymidylate synthesis (26). Interestingly, dUTPase mutations in *Escherichia coli* increased dUTP levels, leading to dUTP misincorporation into DNA during replication, which resulted in DNA fragmentation and apoptosis (27). Furthermore, introduction of *E. coli* dUTPase into human tumour cells resulted in the induction of resistance to fluorodeoxyuridine cytotoxicity (28), suggesting a pivotal role of dUTPase in the prevention of DNA damage. Thus, dUTPase activation in the nucleus appears to be critical

Table 2. Clinicopathological characteristics and dUTP pyrophosphatase expression in hepatocellular carcinoma ($n = 82$)

dUTPase expression (nuclear)	Low ($n = 52$)	High ($n = 30$)	*P*-value
Age (< 60 years/≥60 years)	19/33	8/22	0.36
Sex (male/female)	36/16	23/7	0.47
Virus (HBV/HCV/B+C/NBNC)	15/33/1/3	10/20/0/0	0.48
Cirrhosis (yes/no)	33/19	22/8	0.36
AFP (< 20 ng/ml/≥20 ng/ml)	32/20	15/15	0.31
Histological grade*			
I–II	14	3	
II–III	36	20	
III–IV	2	7	0.0099
Tumour size (< 3 cm/≥3 cm)	31/21	19/11	0.74
TNM classification† (I, II/III, IV)	43/9	25/5	0.94
dUTPase expression (cytoplasmic)	Low ($n = 27$)	High ($n = 55$)	*P*-value
Age (< 60 years/≥60 years)	10/17	17/38	0.58
Sex (male/female)	19/8	40/15	0.82
Virus (HBV/HCV/B+C/NBNC)	8/17/1/1	17/36/0/2	0.56
Cirrhosis (yes/no)	17/10	38/17	0.58
AFP (< 20 ng/ml/≥20 ng/ml)	16/11	31/24	0.80
Histological grade*			
I–II	7	10	
II–III	20	36	
III–IV	0	9	0.077
Tumour size (< 3cm/≥3 cm)	17/10	33/22	0.80
TNM classification† (I, II/III, IV)	21/6	47/8	0.39

*Edmondson–Steiner grades.
†UICC TNM classification of liver cancer, 6th edition (2002).
AFP, α-fetoprotein; dUTPase, dUTP pyrophosphatase; HBV, hepatitis B virus; HCV, hepatitis C virus.

Table 3. Cox regression analysis of recurrence-free survival rate relative to dUTP pyrophosphatase expression and clinicopathological parameters ($n = 82$)

	Univariate		Multivariate	
Variables (n)	HR (95% CI)	*P*-value	HR (95% CI)	*P*-value
Child–Pugh				
A	1			
B	1.73 (0.50–5.97)	0.38		
Tumour size				
< 3 cm ($n = 50$)	1			
≥3 cm ($n = 32$)	1.58 (0.69–3.63)	0.28		
TNM stage*				
I, II ($n = 68$)	1		1	
III, IV ($n = 14$)	2.57 (1.05–6.29)	0.039	2.75 (1.11–6.79)	0.027
Serum AFP				
< 20 ng/ml ($n = 49$)	1			
≥20 ng/ml ($n = 38$)	1.54 (0.66–3.56)	0.31		
Microvascular invasion				
No	1			
Yes	1.98 (0.89–4.44)	0.095		
BCLC stage				
A	1			
B/C	2.16 (0.93–5.00)	0.07		
Cytoplasmic dUTPase				
Low ($n = 27$)	1			
High ($n = 55$)	1.15 (0.50–2.62)	0.73		
Nuclear dUTPase				
Low ($n = 52$)	1		1	
High ($n = 30$)	2.47 (1.08–5.66)	0.032	2.61 (1.13–6.05)	0.024

*UICC TNM classification of liver cancer, 6th edition (2002).
AFP, α-fetoprotein; CI, confidence intervals; dUTPase, dUTP pyrophosphatase; HR, hazard ratio.

for preventing DNA damage possibly at the S phase. Specifically, this activation may prevent dUTP misincorporation in various cancers and thus avert DNA damage and apoptosis induction. Indeed, dUTPase activation has recently been reported in colorectal and brain cancer (29, 30), and dUTPase accumulation might correlate with 5-FU-based chemotherapy resistance and poor prognosis in colorectal cancer (26).

If dUTPase activation plays a central role in the development of resistance to thymidylate synthase inhibitors in order to prevent a DNA damage response, dUTPase inhibition may facilitate the eradication of cancer cells by sensitizing these cells to such inhibitors. Indeed, a recent study suggested a drastic sensitization of colon cancer cells to 5-FU by siRNAs-mediated dUTPase suppression (31, 32), which is consistent with our current observation. Because all HCC samples used in this study were surgically resected, we could not evaluate the effect of dUTPase expression on clinical HCC patients' outcome in relation to chemosensitivity to thymidylate synthase inhibitors. Nevertheless, intense nuclear dUTPase expression may be a good biomarker for predicting the response to thymidylate synthase inhibitors, and its usefulness should be further evaluated in the future.

In conclusion, comprehensive gene expression profiling shed new light on the role of dUTPase in HCC. Nuclear dUTPase accumulation is potentially a good biomarker for predicting poor prognosis in HCC patients, and the development of a dUTPase inhibitor may promote the possibility of tumour eradication in HCC patients.

Acknowledgements

The authors would like to thank Ms Masayo Baba and Nami Nishiyama for technical assistance. This research was supported in part by a Grant-in-Aid for Special Purposes from the Ministry of Education, Culture, Sports, Science and Technology, Japan (no. 20599005).

Grant support: Grant-in-Aid for Special Purposes from the Ministry of Education, Culture, Sports, Science and Technology, Japan (no. 20599005).

References

1. Parkin DM, Bray F, Ferlay J, Pisani P. Global cancer statistics, 2002. *CA Cancer J Clin* 2005; **55**: 74–108.
2. El-Serag HB, Rudolph KL. Hepatocellular carcinoma: epidemiology and molecular carcinogenesis. *Gastroenterology* 2007; **132**: 2557–76.
3. Farazi PA, Depinho RA. Hepatocellular carcinoma pathogenesis: from genes to environment. *Nat Rev Cancer* 2006; **6**: 674–87.
4. Roessler S, Budhu A, Wang XW. Future of molecular profiling of human hepatocellular carcinoma. *Future Oncol* 2007; **3**: 429–39.
5. El-Serag HB, Marrero JA, Rudolph L, Reddy KR. Diagnosis and treatment of hepatocellular carcinoma. *Gastroenterology* 2008; **134**: 1752–63.
6. Llovet JM, Bruix J. Novel advancements in the management of hepatocellular carcinoma in 2008. *J Hepatol* 2008; **48**(Suppl. 1): S20–37.
7. Poon RT, Fan ST, Lo CM, Liu CL, Wong J. Long-term survival and pattern of recurrence after resection of small hepatocellular carcinoma in patients with preserved liver function: implications for a strategy of salvage transplantation. *Ann Surg* 2002; **235**: 373–82.
8. Friedman MA. Primary hepatocellular cancer–present results and future prospects. *Int J Radiat Oncol Biol Phys* 1983; **9**: 1841–50.
9. Lin DY, Lin SM, Liaw YF. Non-surgical treatment of hepatocellular carcinoma. *J Gastroenterol Hepatol* 1997; **12**: S319–28.
10. Nagano H, Miyamoto A, Wada H, *et al.* Interferon-alpha and 5-fluorouracil combination therapy after palliative hepatic resection in patients with advanced hepatocellular carcinoma, portal venous tumor thrombus in the major trunk, and multiple nodules. *Cancer* 2007; **110**: 2493–501.
11. Patt YZ, Hassan MM, Lozano RD, *et al.* Phase II trial of systemic continuous fluorouracil and subcutaneous recombinant interferon alfa-2b for treatment of hepatocellular carcinoma. *J Clin Oncol* 2003; **21**: 421–7.
12. Urabe T, Kaneko S, Matsushita E, Unoura M, Kobayashi K. Clinical pilot study of intrahepatic arterial chemotherapy with methotrexate, 5-fluorouracil, cisplatin and subcutaneous interferon-alpha-2b for patients with locally advanced hepatocellular carcinoma. *Oncology* 1998; **55**: 39–47.
13. Obi S, Yoshida H, Toune R, *et al.* Combination therapy of intraarterial 5-fluorouracil and systemic interferon-alpha for advanced hepatocellular carcinoma with portal venous invasion. *Cancer* 2006; **106**: 1990–7.
14. Honda M, Yamashita T, Ueda T, *et al.* Different signaling pathways in the livers of patients with chronic hepatitis B or chronic hepatitis C. *Hepatology* 2006; **44**: 1122–38.
15. Nishino R, Honda M, Yamashita T, *et al.* Identification of novel candidate tumour marker genes for intrahepatic cholangiocarcinoma. *J Hepatol* 2008; **49**: 207–16.
16. Yamashita T, Honda M, Takatori H, *et al.* Genome-wide transcriptome mapping analysis identifies organ-specific gene expression patterns along human chromosomes. *Genomics* 2004; **84**: 867–75.
17. Yamashita T, Kaneko S, Hashimoto S, *et al.* Serial analysis of gene expression in chronic hepatitis C and hepatocellular carcinoma. *Biochem Biophys Res Commun* 2001; **282**: 647–54.
18. Yamashita T, Honda M, Kaneko S. Application of serial analysis of gene expression in cancer research. *Curr Pharm Biotechnol* 2008; **9**: 375–82.
19. Yamashita T, Honda M, Takatori H, *et al.* Activation of lipogenic pathway correlates with cell proliferation and poor prognosis in hepatocellular carcinoma. *J Hepatol* 2009; **50**: 100–10.
20. Velculescu VE, Zhang L, Vogelstein B, Kinzler KW. Serial analysis of gene expression. *Science* 1995; **270**: 484–7.
21. Yamashita T, Hashimoto S, Kaneko S, *et al.* Comprehensive gene expression profile of a normal human liver. *Biochem Biophys Res Commun* 2000; **269**: 110–6.
22. Polyak K, Xia Y, Zweier JL, Kinzler KW, Vogelstein B. A model for p53-induced apoptosis. *Nature* 1997; **389**: 300–5.
23. Misu H, Takamura T, Matsuzawa N, *et al.* Genes involved in oxidative phosphorylation are coordinately upregulated with fasting hyperglycaemia in livers of patients with type 2 diabetes. *Diabetologia* 2007; **50**: 268–77.
24. Longley DB, Harkin DP, Johnston PG. 5-fluorouracil: mechanisms of action and clinical strategies. *Nat Rev Cancer* 2003; **3**: 330–8.
25. Whitfield ML, George LK, Grant GD, Perou CM. Common markers of proliferation. *Nat Rev Cancer* 2006; **6**: 99–106.
26. Ladner RD, Lynch FJ, Groshen S, *et al.* dUTP nucleotidohydrolase isoform expression in normal and neoplastic tissues: association with survival and response to 5-fluorouracil in colorectal cancer. *Cancer Res* 2000; **60**: 3493–503.
27. El-Hajj HH, Zhang H, Weiss B. Lethality of a dut (deoxyuridine triphosphatase) mutation in *Escherichia coli*. *J Bacteriol* 1988; **170**: 1069–75.
28. Canman CE, Radany EH, Parsels LA, *et al.* Induction of resistance to fluorodeoxyuridine cytotoxicity and DNA damage in human tumor cells by expression of *Escherichia coli* deoxyuridinetriphosphatase. *Cancer Res* 1994; **54**: 2296–8.
29. Fleischmann J, Kremmer E, Muller S, *et al.* Expression of deoxyuridine triphosphatase (dUTPase) in colorectal tumours. *Int J Cancer* 1999; **84**: 614–7.
30. Romeike BF, Bockeler A, Kremmer E, *et al.* Immunohistochemical detection of dUTPase in intracranial tumors. *Pathol Res Pract* 2005; **201**: 727–32.
31. Koehler SE, Ladner RD. Small interfering RNA-mediated suppression of dUTPase sensitizes cancer cell lines to thymidylate synthase inhibition. *Mol Pharmacol* 2004; **66**: 620–6.

32. Wilson PM, Fazzone W, Labonte MJ, *et al.* Novel opportunities for thymidylate metabolism as a therapeutic target. *Mol Cancer Ther* 2008; **7**: 3029–37.

Supporting Information

Additional Supporting Information may be found in the online version of this article:

Fig. S1. Subcellular localization of genes detected in each SAGE library.

Fig. S2. Microarray analysis of *DUT* and *TS* gene expression in 238 HCC cases publicly available (GSE5975). *DUT* was overexpressed more than 2-fold in 121 of 238 HCC tissues (median: 2.03), whereas *TS* was overexpressed more than 2-fold in 54 of 238 HCC tissues (median: 1.41) compared with the non-cancerous liver tissues.

Fig. S3. (A) Transfection of siRNAs targeting *DUT* (DUT2) decreased *DUT* expression compared with the control (scrambled sequence). Gene expression was evaluated in triplicates 72 hours after transfection (mean ± SD). (B) *DUT* gene knockdown sensitized HuH7 cells to low-dose 5-FU (0.25 mg/ml) (mean ± SD).

Fig. S4. Nuclear and cytoplasmic dUTPase expression and cell proliferation in HCC. PCNA indexes in nuclear dUTPase-high HCC were higher than those in -low HCC with statistical significance ($P = 0.01$). Cytoplasmic dUTPase expression was not associated with PCNA indexes in HCC.

Table S1. A summary of constructed SAGE libraries.

Please note: Wiley-Blackwell is not responsible for the content or functionality of any supporting materials supplied by the authors. Any queries (other than missing material) should be directed to the corresponding author for the article.

Genomics 95 (2010) 217–223

Contents lists available at ScienceDirect

Genomics

journal homepage: www.elsevier.com/locate/ygeno

Comprehensive gene expression analysis of 5′-end of mRNA identified novel intronic transcripts associated with hepatocellular carcinoma

Yuji Hodo [a], Shin-ichi Hashimoto [b], Masao Honda [a], Taro Yamashita [a], Yutaka Suzuki [c], Sumio Sugano [c], Shuichi Kaneko [a,*], Kouji Matsushima [b]

[a] Department of Gastroentelorogy, Kanazawa University Graduate School of Medical Science, 13-1 Takara-Machi, Kanazawa, Ishikawa 920-8641, Japan
[b] Department of Molecular Preventive Medicine, School of Medicine, The University of Tokyo, 7-3-1, Hongo, Bunkyo-ku, Tokyo 113-0033, Japan
[c] Department of Medical Genome Sciences, Graduate School of Frontier Sciences, The University of Tokyo, 5-1-5, Kashiwanoha, Kashiwa, Chiba 277-8562, Japan

ARTICLE INFO

Article history:
Received 1 June 2009
Accepted 14 January 2010
Available online 21 January 2010

Keywords:
5′-end serial analysis of gene expression
Transcriptional start site
Acyl-coenzyme A oxidase 2
Intron
Hepatocellular carcinoma

ABSTRACT

To elucidate the molecular feature of human hepatocellular carcinoma (HCC), we performed 5′-end serial analysis of gene expression (5′SAGE), which allows genome-wide identification of transcription start sites in addition to quantification of mRNA transcripts. Three 5′SAGE libraries were generated from normal human liver (NL), non-B, non-C HCC tumor (T), and background non-tumor tissues (NT). We obtained 226,834 tags from these libraries and mapped them to the genomic sequences of a total of 8,410 genes using RefSeq database. We identified several novel transcripts specifically expressed in HCC including those mapped to the intronic regions. Among them, we confirmed the transcripts initiated from the introns of a gene encoding acyl-coenzyme A oxidase 2 (*ACOX2*). The expression of these transcript variants were up-regulated in HCC and showed a different pattern compared with that of ordinary *ACOX2* mRNA. The present results indicate that the transcription initiation of a subset of genes may be distinctively altered in HCC, which may suggest the utility of intronic RNAs as surrogate tumor markers.

Introduction

Hepatocellular carcinoma (HCC) is the fifth most common cancer worldwide and the third most common cause of cancer mortality. HCC usually develops in patients with virus-induced (e.g., hepatitis B virus (HBV) and hepatitis C virus (HCV)) chronic inflammatory liver disease [1]; however, non-B, non-C HCC has been reported in patients negative for both HBV and HCV [2]. HCC development is a multistep process involving changes in host gene expression, some of which are correlated with the appearance and progression of a tumor. Multiple studies linking hepatitis viruses and chemical carcinogens with hepatocarcinogesis have provided insights into tumorigenesis [1,3]. Nevertheless, the genetic events that lead to HCC development remain unknown, and the molecular pathogenesis of HCC in most patients is still unclear. Therefore, elucidation of the genetic changes specific to the pathogenesis of non-B, non-C HCC may be useful to reveal the molecular features of HCCs irrelevant to viral infection.

Gene expression profiling, either by cDNA microarray [4] or serial analysis of gene expression (SAGE) [5], is a powerful molecular technique that allows analysis of the expression of thousands of genes. In particular, SAGE enables the rapid, quantitative, and simultaneous monitoring of the expression of tens of thousands of genes in various tissues [6,7]. Although numerous studies using cDNA microarrays and SAGE have been performed to clarify the genomic and molecular alterations associated with HCC [6,8–10], most expression data have been derived from the 3′-end region of mRNA. Recent advances in molecular biology have enabled genome-wide analysis of the 5′-end region of mRNA that revealed the variation in transcriptional start sites [11,12] and the presence of a large number of non-coding RNAs [13]. These approaches might be useful for identifying the unique and undefined genes associated with HCC not identified by the analysis of the 3′-end region of mRNA. SAGE based on the 5′-end (5′SAGE), a recently developed technique, allows for a comprehensive analysis of the transcriptional start site and quantitative gene expression [14]. This article is to elucidate the molecular carcinogenesis of non-B, non-C HCCs, while those heterogeneous entities are supposed not to share the same etiology, by using 5′SAGE.

Results

Annotation of the 5′SAGE tags to the human genome

We characterized a total of 226,834 tags from three unique 5′SAGE libraries (75,268 tags from the normal liver (NL) library, 75,573 tags from the non-tumor tissue (NT) library, and 75,993 tags from the tumor (T) library) and compared them against the human genome

Abbreviations: 5′SAGE, 5′-end serial analysis of gene expression; HCC, hepatocellular carcinoma; ACOX2, acyl-coenzyme A oxidase 2.

* Corresponding author. Fax: +81 76 234 4250
E-mail address: skaneko@m-kanazawa.jp (S. Kaneko).

0888-7543/$ – see front matter © 2010 Elsevier Inc. All rights reserved.
doi:10.1016/j.ygeno.2010.01.004

sequence. A total of 211,818 tags matched genomic sequences, representing 104,820 different tags in the three libraries (Table 1). About 60–65% of these tags mapped to a single locus in the genome in each library. Then, we mapped these single-matched tags to the well-annotated genes using RefSeq database (www.ncbi.nlm.nih.gov/RefSeq/, reference sequence database developed by NCBI). A total of 45,601 tags from the NL library, 39,858 from the NT library, and 41,265 from the T library were successfully mapped to 8410 unique genes (4397 genes detected in the NL library, 5194 genes in the NT library, and 6304 genes in the T library).

Gene expression profiling of non-B, non-C HCC

Abundantly expressed transcripts in the NL library and their corresponding expression in the NT and T libraries are shown in Table 2. The most abundant transcript in all three libraries was encoded by the *albumin (ALB)* gene. Transcripts encoding apolipoproteins were also abundantly expressed in each library, suggesting the preservation of hepatocytic gene expression patterns in HCC. Of note, the expression of *haptoglobin (HP)* (NL: 631, NT: 329, T: 57) and *metallothionein 1G (MT1G)* (NL: 392, NT: 169, T: 2) was decreased in the NT library and more in T library compared with NL library. Furthermore, the expression of *metallothionein 2A (MT2A)* (NL: 1027, NT: 872, T: 19), *metallothionein 1X (MT1X)* (NL: 547, NT: 644, T: 11), and *metallothionein 1E (MT1E)* (NL: 275, NT: 340, T: 2) was decreased almost fifty-fold or more in the T library compared with the NL and NT libraries. In contrast, the expression of *ribosomal protein S29 (RPS29)* (NL: 372, NT: 1011, T: 1768) was increased in the NT library and more in T library compared with NL library. Thus, transcripts associated with a certain liver function including xenobiotic metabolism might be suppressed whereas those associated with protein synthesis might be expressed in non-B, non-C HCC, similar to that observed in HCV-HCC [15].

We then investigated the characteristics of gene expression patterns in non-B, non C HCC. Two hundred fifty-four and 172 genes were up- or down-regulated in the T library more than five-fold compared with the NL library (data not shown). The top 10 genes are listed in Table 3a, and we identified several novel genes not yet reported to be differentially expressed in non-B, non-C HCC. Representative novel gene expression changes identified by 5′SAGE were validated by semi-quantitative reverse transcriptase-polymerase chain reaction (RT-PCR) analysis (Supplemental Fig. 1). RT-PCR results showed that the expression of *galectin 4 (LGALS4)*, *X antigen family, member 1A (XAGE 1A)*, *retinol dehydrogenase 11 (RDH11)*, *hydroxysteroid (17-beta) dehydrogenase 14 (HSD17B14)* *transmembrane 14A (TMEM14A)*, *stimulated by retinoic acid 13 homolog (STRA13)*, and *dual specificity phosphatase 23 (DUSP23)* was increased, whereas the expression of *C-type lectin superfamily 4 member G (CLEC4G)* was decreased in HCC tissues compared with the non-tumor tissues.

To further characterize the gene expression patterns of non-B, non-C HCC comprehensively, we compared the Gene Ontology process of three types of HCCs (i.e., non-B, non-C HCC; HBV-HCC; HCV-HCC) based on our previously described data [16]. The pathway analysis using MetaCore™ software showed that the immune related and cell adhesion related pathways were up-regulated in HCV-HCC with statistically significance, and the insulin signaling and angiogenesis related pathways were up-regulated in HBV-HCC with statistically significance, confirming our previous results [16]. Interestingly, genes associated with progesterone signaling were up-regulated in non-B, non-C HCC, while genes associated with proteolysis in the cell cycle, apoptosis and the ESR1-nuclear pathway were up-regulated in all types of HCC (Supplemental Fig. 2).

Dynamic alteration of transcription initiation in HCC

Although various transcriptome analyses have discovered considerable gene expression changes in cancer, it is still unclear if transcription is differentially initiated and/or terminated in HCC compared with the non-cancerous liver. We therefore explored the characteristics of transcription initiation and/or termination in HCC using 5′SAGE and 3′SAGE data. Markedly, we observed relevant differences between 5′ SAGE and 3′SAGE data derived from the same HCC sample (Tables 3a and b). For example, a gene encoding *coagulation factor XIII, B polypeptide (F13B)* was 13-fold up-regulated at transcription start sites (5′SAGE) but two-fold down-regulated at transcription termination sites (3′SAGE). On the other hand, a gene encoding *adenylate cyclase 1 (ADCY1)* was 50-fold down-regulated at transcriptional termination sites (3′SAGE) but showed no difference at transcriptional start sites (5′SAGE). These data suggest the dramatic alteration of all process of transcription in HCC, and the transcripts initiated at certain sites might be specifically associated with and involved in HCC pathogenesis, which could be a novel marker for HCC diagnosis.

Identification of novel intronic transcripts in HCC

Recent lines of evidence suggest that the majority of sequences of eukaryotic genomes may be transcribed, not only from known transcription start sites but also from intergenic regions and introns [17,18]. Introns are recognized as a significant source of functional non-coding RNAs (ncRNAs) including microRNAs (miRNAs) [18]. Moreover, a recent report implied the role of some large intronic RNAs in the pathogenesis of several types of malignancies [19]. Thus, analysis of transcripts originating from introns might be valuable for elucidating the genetic traits of HCC. We therefore focused on the transcriptional start sites potentially initiated from the intron and deregulated in HCC using 5′SAGE data. We identified that 97% of 5′ SAGE tags annotated by the RefSeq database matched the sequences in the exons, while 3% matched those in the introns (1257 in the N library, 1225 in the NT library, and 1261 in the T library) (Table 4a). To identify the possible promoter regions located in the intron, we clustered the different SAGE tags to a certain genomic region if these tags positioned within 500 bp intervals (Supplemental Fig. 3), as described previously [12].

Table 1
Experimental matching of 5′SAGE tags to genome.

	Normal liver	Non-tumor	Tumor	Total
All tags	75,268	75,573	75,993	226,834
Tags mapped to genome (%)				
1 locus/genome	51,076 (71.2)	47,200 (68.0)	48,503 (68.5)	146,779 (69.3)
Multiple loci/genome	20,608 (28.8)	22,142 (32.0)	22,289 (31.5)	65,039 (30.7)
Total tags	71,684 (100)	69,342 (100)	70,792 (100)	211,818 (100)
Unique tags mapped to genome (%)				
1 locus/genome	20,736 (65.5)	20,487 (60.2)	23,753 (60.7)	64,976 (62.0)
Multiple loci/genome	10,914 (34.5)	13,548 (39.8)	15,382 (39.3)	39,844 (38.0)
Total tags	31,650 (100)	34,035 (100)	39,135 (100)	104,820 (100)
Total tags to RefSeq	45,601	39,858	41,265	126,724
Unique gene	4397	5194	6304	8410

5′SAGE indicates 5′-end serial analysis of gene expression.

Table 2
The highly expressed genes in the NL library and corresponding expression in the NT and T libraries (top 50 from NL library).

Tag count			Ratio		Gene
NL	NT	T	NT/NL	T/NL	
3731	1716	2328	0.460	0.624	Albumin (ALB)
2484	2146	2042	0.864	0.822	Apolipoprotein C-I (APOC1)
1955	1603	1079	0.820	0.552	Apolipoprotein A-II (APOA2)
1653	1050	828	0.635	0.501	Apolipoprotein A-I (APOA1)
1252	1908	1203	1.524	0.961	Transthyretin (prealbumin, amyloidosis type I) (TTR)
1233	724	220	0.587	0.178	Serpin peptidase inhibitor, clade A, member 1 (SERPINA1)
1027	872	19	0.849	0.019	Metallothionein 2A (MT2A)
755	1144	762	1.515	1.009	Ferritin, light polypeptide (FTL)
713	632	680	0.886	0.954	Alpha-1-microglobulin/bikunin precursor (AMBP)
635	524	1336	0.825	2.104	Apolipoprotein E (APOE)
631	329	57	0.521	0.090	Haptoglobin (HP)
600	228	212	0.380	0.353	Fibrinogen gamma chain (FGG)
549	395	302	0.719	0.550	Apolipoprotein C-III (APOC3)
547	644	11	1.177	0.020	Metallothionein 1X (MT1X)
479	257	290	0.537	0.605	Tumor protein, translationally-controlled 1 (TPT1)
463	217	53	0.469	0.114	Serpin peptidase inhibitor, clade A, member 3 (SERPINA3)
393	204	206	0.519	0.524	Ribosomal protein L26 (RPL26)
392	169	2	0.431	0.005	Metallothionein 1G (MT1G)
372	1011	1768	2.718	4.753	Ribosomal protein S29 (RPS29)
306	163	223	0.533	0.729	Ribosomal protein S27 (RPS27)
279	135	159	0.484	0.570	Ribosomal protein S16 (RPS16)
275	340	2	1.236	0.007	Metallothionein 1E (MT1E)
269	170	246	0.632	0.914	Ribosomal protein S23 (RPS23)
260	142	92	0.546	0.354	Fibrinogen beta chain (FGB)
260	200	195	0.769	0.750	Aldolase B, fructose-bisphosphate (ALDOB)
255	228	286	0.894	1.122	Ribosomal protein S12 (RPS12)
248	162	198	0.653	0.798	Ribosomal protein S14 (RPS14)
246	175	70	0.711	0.285	Interferon induced transmembrane protein 3 (IFITM3)
239	198	273	0.828	1.142	Ribosomal protein L31(RPL31)
229	264	0	1.153	0.004	Hepcidin antimicrobial peptide (HAMP)
228	149	156	0.654	0.684	Ribosomal protein S20 (RPS20)
222	191	117	0.860	0.527	Ubiquitin B (UBB)
216	218	352	1.009	1.630	Ribosomal protein L41 (RPL41)
210	150	155	0.714	0.738	Ribosomal protein, large, P1(RPLP1)
201	110	90	0.547	0.448	Ribosomal protein, large, P2 (RPLP2)
198	102	64	0.515	0.323	Fibrinogen alpha chain (FGA)
196	143	408	0.730	2.082	Ribosomal protein L37 (RPL37)
192	123	56	0.641	0.292	Ribosomal protein L37a (RPL37A)
191	208	346	1.089	1.812	Ribosomal protein L30 (RPL30)
174	109	76	0.626	0.437	Ribosomal protein L35 (RPL35)
169	208	3	1.231	0.018	Cytochrome P450, family 2, subfamily E, polypeptide 1 (CYP2E1)
167	105	300	0.629	1.796	Apolipoprotein H (beta-2-glycoprotein I) (APOH)
162	106	33	0.654	0.204	Serum amyloid A4, constitutive (SAA4)
159	85	157	0.535	0.987	Ribosomal protein L34 (RPL34)
159	113	229	0.711	1.440	Transferrin (TF)
155	84	135	0.542	0.871	Ribosomal protein S11 (RPS11)
152	125	101	0.822	0.664	Ribosomal protein S13 (RPS13)
147	84	1	0.571	0.007	Nicotinamide *N*-methyltransferase (NNMT)
147	180	35	1.224	0.238	Hemopexin (HPX)
146	89	121	0.610	0.829	Alpha-2-HS-glycoprotein (AHSG)

To avoid division by 0, a tag value of 1 for any tag that was not detectable was used.
NL, normal liver; NT, non-tumor; T, tumor.

More than 2 tags were detected in the intronic regions of the 164 genes in the NL, 168 genes in the NT, and 157 genes in the T library, suggesting that these regions might be potential intronic promoter regions (Table 4a). The biological process of these intron-origin transcripts using Human Protein Reference Database (http://www.hprd.org/) showed that these were related to basic cellular functions such as signal transduction, transport, and regulation of the nucleobase and nucleotide, suggesting that these intronic transcripts may play a fundamental role in the liver (data not shown). Among these genes, 12 were differentially expressed between the NL and T libraries more than four-fold (Table 4b). Interestingly, intronic transcripts (determined by 5′SAGE) of genes encoding *SAMD3*,

Table 3a
Differentially expressed genes in HCC (top 10 from 5′SAGE).

5′SAGE	3′SAGE	5′/3′	Gene
T/NL	T/NL	Ratio	
Up-regulated gene			
19	6	3.17	P antigen family, member 2 (prostate associated) (PAGE2)
18	10	1.8	Lectin, galactoside-binding, soluble, 4 (LGALS4)
16	3	5.33	Choline phosphotransferase 1 (CHPT1)
14	2	7	X antien family, member 1A (XAGE1A)
14	2	7	Dehydrogenase/reductase (SDR family) member 4 (DHRS4)
14	2	7	Sterol-C5-desaturase-like (SC5DL)
13	0.5	26	Coagulation factor XIII, B polypeptide (F13B)
13	2.33	5.58	Retinol dehydrogenase 11 (all-trans and 9-cis) (RDH11)
13	0.5	26	Transmembrane protein 14A (TMEM14A)
12	1.33	9.02	Dual specificity phosphatase 23 (DUSP23)
Down-regulated gene			
0.00436	0.0137	0.318	Hepcidin antimicrobial peptide (HAMP)
0.0051	ND		Metallothionein 1G (MT1G)
0.0068	0.04	0.17	Nicotinamide *N*-methyltransferase (NNMT)
0.00727	ND		Metallothionein 1E (functional) (MT1E)
0.0098	0.0526	0.186	C-reactive protein, pentraxin-related (CRP)
0.0145	ND		Metallothionein 1 M (MT1M)
0.0152	ND		Phospholipase A2, group IIA (platelets, synovial fluid) (PLA2G2A)
0.0178	0.111	0.16	Cytochrome P450, family 2, subfamily E, polypeptide 1 (CYP2E1)
0.0185	0.192	0.096	Metallothionein 2A (MT2A)
0.0201	ND		Metallothionein 1X (MT1X)

3′SAGE, 3′-end serial analysis of gene expression; 5′SAGE, 5′-end serial analysis of gene expression; HCC, hepatocellular carcinoma; NL, normal liver; T, tumor.

Table 3b
Differentially expressed genes in HCC (top 10 from 3′SAGE).

5′SAGE	3′SAGE	5′/3′	Gene
T/NL	T/NL	Ratio	
Up-regulated gene			
ND	15		Leukocyte immunoglobulin-like receptor, subfamily B, member 1 (LILRB1)
ND	12		Fibroblast growth factor 5 (FGF5)
1	11	0.909	Adenosine deaminase, tRNA-specific 1 (ADAT1)
5	11	0.454	px19-like protein (PRELID1)
4.4	11	0.4	Anaphase promoting complex subunit 11 (ANAPC11)
ND	10.3		Chromosome 21 open reading frame 77 (C21orf77)
ND	10		von Willebrand factor (VWF)
2.333	10	0.233	ATX1 antioxidant protein 1 homolog (yeast) (ATOX1)
18	10	1.8	Lectin, galactoside-binding, soluble, 4 (LGALS4)
ND	9.5		Solute carrier family 26 (sulfate transporter), member 2 (SLC26A2)
Down-regulated gene			
0.5	0.012	41.7	ELL associated factor 1 (EAF1)
0.5	0.0137	36.5	TGF beta-inducible nuclear protein 1 (NSA2)
0.000436	0.0137	0.032	Hepcidin antimicrobial peptide (HAMP)
1	0.0179	55.9	Basic, immunoglobulin-like variable motif containing (BIVM)
ND	0.0182		DNA fragmentation factor, 45 kDa, alpha polypeptide (DFFA)
1	0.0185	54.1	GRIP1 associated protein 1 (GRIPAP1)
ND	0.0189		Nuclear factor of activated T-cells 5, tonicity-responsive (NFAT5)
1	0.0204	49	Adenylate cyclase 1 (ADCY1)
0.333	0.0312	10.7	Dihydroorotate dehydrogenase (DHODH)
0.738	0.0312	23.7	Ribosomal protein, large, P1 (RPLP1)

3′SAGE, 3′-end serial analysis of gene expression; 5′SAGE, 5′-end serial analysis of gene expression; HCC, hepatocellular carcinoma; NL, normal liver; T, tumor.

Table 4a
Number of 5′SAGE tags mapped to intronic region.

	NL	NT	T
Tag mapped to intron	1287	1253	1292
Total promoter region	952	981	1020
(tag number = 1)	788	813	863
(tag number ≧2)	164	168	157

ACOX2, *HGD*, *CYP3A5*, *KNG1* and *AGXT* were increased, while their 3′ transcripts (determined by 3′SAGE) were decreased in HCC. In contrast, both 5′ intronic transcripts and 3′ transcripts encoding *HFM1*, *SERPINA1*, *SUPT3H*, *A2M* and *TMEM176B* were similarly decreased in HCC. Taken together, these data imply that the canonical- and intronic-promoter activities of a subset of genes including *SAMD3*, *ACOX2*, *HGD*, *CYP3A5*, *KNG1* and *AGXT* might be differently regulated in HCC.

ACOX2 as a novel intronic gene deregulated in HCC

A subset of genes listed above may be transcribed from intronic regions specifically in HCC. Among these genes, we focused on the regulation of *ACOX2*, which is reported to be potentially involved in peroxisomal beta-oxidation and hepatocarcinogenesis [20]. The intron-origin expression of *ACOX2* increased six-fold in HCC compared with the NT by 5′SAGE, while the expression based on the 3′end was almost similar between HCC and NT lesions (Table 4b). Close examination of 5′SAGE data identified two potential intron-origin transcripts of *ACOX2* (Supplemental Fig. 4). The first (intronic-*ACOX2-1*) was initiated upstream of the tenth exon, whereas the second (intronic-*ACOX2-2*) was initiated upstream of the twelfth exon of *ACOX2* (Supplemental Fig. 4). The sequence of the intronic part was unique, and the remaining part of the sequence was shared with the canonical transcripts of *ACOX2*.

The expression of canonical *ACOX2* and the two types of intron-origin transcripts was investigated in NL, NT, and T tissues by RT-PCR (Fig. 1A). Although canonical *ACOX2* expression was decreased in T than in NL, the intron-origin transcript, particularly intronic-*ACOX2-1*, was increased in T. Intronic-*ACOX2-2* transcripts also showed a modest increase. We further evaluated the alteration of these transcripts in 19 HBV-HCCs, 20 HCV-HCCs, and 4 non-B, non-C HCCs, and their background liver tissues by canonical *ACOX2* and intronic-*ACOX2* specific real-time detection (RTD)-PCR. Although the expression of canonical *ACOX2* was decreased, the expression of intronic-*ACOX2* was significantly increased (Fig. 1B). Importantly, the gene expression ratios of intronic-to canonical *ACOX2* increased more in moderately differentiated HCCs (mHCC) than in well-differentiated HCCs (wHCC), suggesting the involvement of intronic-*ACOX2* expression on HCC progression.

Table 4b
Differentially expressed intronic promoter regions in HCC.

5′SAGE T/NL	3′SAGE T/NL	5′/3′ Ratio	Gene
Up-regulated			
9	1	9.00	Sterile alpha motif domain containing 3 (SAMD3)
6	0.89	6.74	Acyl-Coenzyme A oxidase 2, branched chain (ACOX2)
6	0.62	9.68	Homogentisate 1,2-dioxygenase (homogentisate oxidase) (HGD)
6	0.009	666.67	Cytochrome P450, family 3, subfamily A, polypeptide 5 (CYP3A5)
5	0.64	7.81	Kininogen 1 (KNG1)
4	0.36	11.11	Alanine-glyoxylate aminotransferase (AGXT)
4	1	4.00	Crystallin, alpha A (CRYAA)
Down-regulated			
0.13	1	0.13	HFM1, ATP-dependent DNA helicase homolog (*S. cerevisiae*) (HFM1)
0.25	0.51	0.49	Serpin peptidase inhibitor, clade A member 1 (SERPINA1)
0.25	1	0.25	Suppressor of Ty 3 Homolog (*S. cerevisiae*) (SUPT3H)
0.25	0.2	1.25	Alpha-2-macroglobulin (A2M)
0.25	0.083	3.13	Transmembrane protein 176B (TMEM176B)

3′SAGE, 3′-end serial analysis of gene expression; 5′SAGE, 5′-end serial analysis of gene expression; HCC, hepatocellular carcinoma; NL, normal liver; NT, non-tumor; T, tumor.

Discussion

This is the first comprehensive transcriptional analysis of tissue lesions of non-B, non-C HCC, background liver and NL using the 5′ SAGE method. Approximately 6.7% of our 5′SAGE tags showed no matching within the human genome, possibly due to the presence of a single nucleotide polymorphism (SNP) in the human genome. Out of the complete matched tags in the genome, 70% were assigned to unique positions and 30% to two or more loci. The tags with multiple matches with genomic loci were largely retrotransposon elements, repetitive sequences, and pseudogenes.

In this study, the analysis of non-B, non-C HCC enabled us to evaluate direct molecular changes associated with HCC without any bias of gene induction by virus infection. The gene expression profile based on our 5′SAGE tags revealed that *albumin (ALB)* and apolipoproteins were highly expressed in NL, indicating the massive production of plasma proteins in NL; these results are similar to those of our previous study using 3′SAGE [6]. Other genes such as *aldolase B (ALDOB)*, *antitrypsin (SERPINA1)*, and *haptoglobin (HP)* were also highly expressed in NL, in both the 5′SAGE and 3′SAGE libraries (Table 2) [6]. Comparison of the expression profiles among NL, background NT and T identified several differentially expressed transcripts in T. *Galectin-4 (LGALS4)* was up-regulated and *HAMP*, *NNMT*, *CYP2E1*, and *metallothionein* were down-regulated in HCC in accordance with previous findings (Table 3a) [8,9,21]. Moreover, *CLEC4G*, which was predominantly expressed in the sinusoidal endothelial cells of the liver, was down-regulated in HCC. In addition, we first found that *P antigen family, member 2 (PAGE2)* and *XAGE1A* were up-regulated in HCC (Table 3a, Supplemental Fig. 1). These genes were members of cancer-testis antigen that include MAGE-family genes. MAGE-family members were originally found to be up-regulated in HCV-related HCC, and reported to be useful as molecular markers and as possible target molecules for immunotherapy in human HCC [22]. In this study, we identified that these members of genes were also up-regulated in non B, non-C HCC. Thus, these genes may be useful as molecular markers and therapeutic targets for the treatment of a certain type of human HCC.

There existed some discrepancy between 5′SAGE and 3′SAGE results, even though they were derived from the same sample. Technical issues such as amplication error, difference of restriction enzyme, and annotation error have been described previously [14]. It is possible that 3′ transcripts might be more stable than 5′ transcripts by binding of ribosomal proteins during translation. Another possibility is the diversity of the transcriptional start and/or termination sites. One of the advantages of 5′SAGE analysis is the potential to determine the transcriptional start sites in each gene. Indeed, a recent study indicated the importance of an insulin splice variant in the pathogenesis of insulinomas [23]. Considering the diversity of 5′ends of genes, it is more appropriate to perform 5′SAGE in combination with 3′SAGE when determining the frequency of gene expression and identifying novel transcript variants.

Here, we were able to identify at least 12 intron-origin transcripts that were differentially expressed in HCC compared with the background liver or NL. These transcripts could not be identified by the 3′SAGE approach. We also performed detailed expression analysis of *ACOX2* that was involved in the beta-oxidation of peroxisome. We

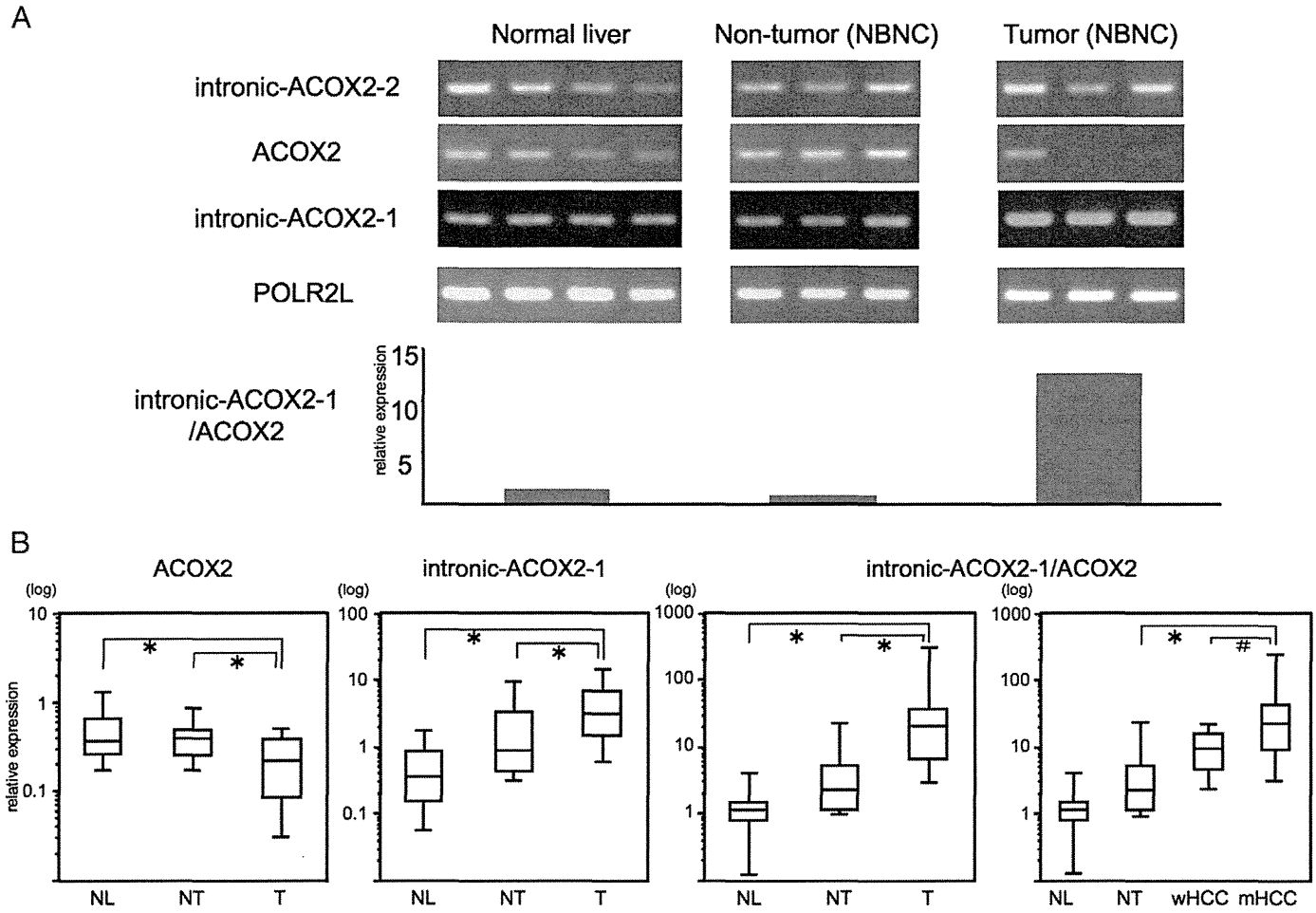

Fig. 1. (A) RT-PCR results of *ACOX2* and *ACOX2* intronic RNAs in independent NL, NT (non-B, non-C), and T (non-B, non-C) samples. RT-PCR was performed in triplicate for each sample-primer set from cDNA. The PCR products were semi-quantitatively analyzed with ImageJ software and calculated as levels relative to *polymerase (RNA) II (DNA directed) polypeptide L* (*POLR2L*). The bar graph indicates the expression ratio of intronic-ACOX2-1 to canonical ACOX2. The expression pattern of intron 1 was different from that of canonical *ACOX2*. (B) RTD-PCR analysis of *ACOX2* and *ACOX2* intronic RNAs in NL, T (HBV-related, HCV-related, and non-B, non-C), and NT tissues. Quantitative RTD-PCR was performed in duplicate for each sample-primer set from cDNA. Each sample was normalized relative to *POLR2L*. All HCC tissues were pathologically diagnosed as well differentiated HCC (wHCC) or moderately differentiated HCC (mHCC). Kruskal–Wallis tests and Mann–Whitney *U* tests were used for statistical analysis. ACOX2, acyl-Coenzyme A oxidase 2; HCC, hepatocellular carcinoma; NL, normal liver; NT, non-tumor; RT-PCR, reverse transcriptase-polymerase chain reaction; RTD-PCR, real-time detection-PCR; T, tumor. $^{*}P<0.01$, $\#P<0.05$.

were able to clone the intron-origin *ACOX2* RNAs (intronic-*ACOX2-1, 2*) for the first time and found that intronic-*ACOX2-1* was significantly overexpressed in T compared with NT and NL. The ratio of intronic-*ACOX2-1* and canonical *ACOX2* (relative intronic-*ACOX2*) was progressively up-regulated from NL via the background liver to HCC. Importantly, the expression of relative intronic-*ACOX2* was more up-regulated in moderately differentiated HCC than in well-differentiated HCC. The intronic difference in expression might be due to a polymorphism, since the 5′SAGE library for NL and T were from different people. The mechanisms of stepwise increase of intronic-*ACOX2* in the process of hepatocarinogenesis should be clarified in future.

ACOX2 is a rate-limiting enzyme of branched-chain acyl-CoA oxidase involved in the degradation of long branched fatty acid and bile acid intermediates in peroxisomes. *ACOX2* expression was associated with the differentiation state of hepatocytes and was repressed under the undifferentiated phase of human hepatoma cell lines [24]. A decreased *ACOX2* expression was also reported in prostate cancer [25]. Here, the expression of canonical *ACOX2* was decreased, while that of intronic-*ACOX2-1* was increased in HCC. The deduced amino acid of intronic-*ACOX2-1* encodes the C-terminal (from 386 to 681 amino acids) of canonical *ACOX2*, lacking the active sites for FAD binding and a fatty acid as the substrate, suggesting that the protein may be functionally departed [26]. The biological role of the increased intronic-*ACOX2-1* was not clear, but it might be reflected by the activation of peroxisome proliferators-activated receptor alpha (PPARA). It is reported that mice lacking ACOX1, another rate-limiting enzyme in peroxisomal straight-chain fatty acid oxidation, developed steatosis and HCC characterized by increased mRNA and protein expression of genes regulated by PPARα [27]. The importance of PPARα activation in HCC development has been recently reported using HCV core protein transgenic mice [28]. Moreover, the overexpression of alpha-methylacyl-CoA racemase (AMACR), an enzyme for branched-chain fatty acid beta-oxidation, is reported to be a reliable diagnostic marker of prostate cancer and is associated with the decreased expression of ACOX2 [25]. Therefore, the expression of intronic-*ACOX2-1* might open the door for further investigations of their potential clinical use, e.g., serving as diagnostic markers of HCC, although the functional relevance of this gene should be further clarified.

In conclusion, we report the first comprehensive transcriptional analysis of non-B, non-C HCC, NT background liver, and NL tissue, based on 5′SAGE. This study offers new insights into the transcriptional changes that occur during HCC development as well as the molecular mechanism of carcinogenesis in the liver. The results suggest the presence of unique intron-origin RNAs that are useful as diagnostic markers and may be used as new therapeutic targets.

Material and methods

Samples

Samples were obtained from a 56-year-old man who had undergone surgical hepatic resection for the treatment of solitary HCC. Serological tests for hepatitis B surface (HBs) antigen and anti-HCV antibodies were negative. Tumor (T) and non-tumor (NT) tissue samples were separately obtained from the tumorous parts (diagnosed as moderately differentiated HCC) and non-tumorous parts (diagnosed as mild chronic hepatitis: F1A1) of the resected tissue. We also obtained five normal liver (NL) tissue samples from five patients who had undergone surgical hepatic resection because of metastatic liver cancer. None of the patients was seropositive for both HBs antigen and anti-HCV antibodies. Neither heavy alcohol consumption nor the intake of chemical agents was observed before surgical resection. All laboratory values related to hepatic function were within the normal range. All procedures and risks were explained verbally and provided in a written consent form.

We additionally used independent four NL tissue samples, 19 HBV-HCCs, 20 HCV-HCCs and 4 non-B, non-C HCCs, and their background liver tissue samples for reverse transcriptase-polymerase chain reaction (RT-PCR) and real-time detection (RTD)-PCR (Supplemental Table 1). Four non-B, non-C HCCs were histologically diagnosed as moderately differentiated HCCs, and the adjacent non-cancerous liver tissues were diagnosed as a normal liver, a chronic hepatitis, a pre-cirrhotic liver and a cryptogenic liver cirrhosis, respectively. None of the patients was seropositive for HBs antigen, anti-HBs antibodies, anti-hepatitis B core (HBc) antibodies and anti-HCV antibodies. Neither heavy alcohol consumption nor the intake of chemical agents was observed. Histological grading of the tumor was evaluated by two independent pathologists as described previously [16].

Generation of the 5′ SAGE library

5′SAGE libraries were generated as previously described [14]. Five to ten micrograms of poly(A)+RNA was treated with bacterial alkaline phosphatase (BAP; TaKaRa, Otsu, Japan). Poly(A)+RNA was extracted twice with phenol: chloroform (1:1), ethanol precipitated, and then treated with tobacco acid pyrophosphatase (TAP). Two to four micrograms of the BAP-TAP-treated poly(A)+RNA was divided into two aliquots and an RNA linker containing recognition sites for *Eco*RI/*Mme*I was ligated using RNA ligase (TaKaRa): one aliquot was ligated to a 5′-oligo 1 (5′-GGA UUU GCU GGU GCA GUA CAA CGA AUU CCG AC-3′) linker, and the other aliquot was ligated to a 5′-oligo 2 (5′-CUG CUC GAA UGC AAG CUU CUG AAU UCC GAC-3′) linker. After removing unligated 5′-oligo, cDNA was synthesized using RNaseH-free reverse-transcriptase (Superscript II, Invitrogen, Carlsbad, CA, USA) at 12 °C for 1 h and 42 °C for the next hour, using 10 pmol of dT adapter-primer (5′-GCG GCT GAA GAC GGC CTA TGT GGC CTT TTT TTT TTT TTT TTT-3′). After first-strand synthesis, RNA was degraded in 15 mM NaOH at 65 °C for 1 h. cDNA was amplified in a volume of 100 μl by PCR with 16 pmol of 5′ (5′ [biotin]-GGA TTT GCT GGT GCA GTA CAA-3′ or 5′[biotin]-CTG CTC GAA TGC AAG CTT CTG-3′) and 3′ (5′-GCG GCT GAA GAC GGC CTA TGT-3′) PCR primers. cDNA was amplified using 10 cycles at 94 °C for 1 min, 58 °C for 1 min, and 72 °C for 2 min. PCR products were digested with the *Mme*I type IIS restriction endonuclease (NEB, Pickering, Ontario, Canada). The digested 5′-terminal cDNA fragments were bound to streptavidin-coated magnetic beads (Dynal, Oslo, Norway). cDNA fragments that bound to the beads were directly ligated together in a reaction mixture containing T4 DNA ligase in a supplied buffer for 2.5 h at 16 °C. The ditags were amplified by PCR using the following primers: 5′ GGA TTT GCT GGT GCA GTA CA 3′ and 5′ CTG CTC GAA TGC AAG CTT CT 3′. The PCR products were analyzed by polyacrylamide gel electrophoresis (PAGE) and digested with *Eco*RI. The region of the gel containing the ditags was excised and the fragments were self-ligated to produce long concatamers that were then cloned into the *Eco*RI site of pZero 1.0 (Invitrogen). Colonies were screened by PCR using the M13 forward and reverse primers. PCR products containing inserts of more than 600 bp were sequenced with Big Dye terminator ver.3 and analyzed using a 3730 ABI automated DNA sequencer (Applied Biosystems, Foster City, CA, USA). All electrophoretograms were reanalyzed by visual inspection to check for ambiguous bases and to correct misreads. In this study, we obtained 19–20 bp tag information.

Association of the 5′SAGE tags with their corresponding genes

We attempted to align our 5′tags with the human genome (NCBI build 36, available from http://www.genome.ucsc.edu/) using the alignment program ALPS (http://www.alps.gi.k.u-tokyo.ac.jp/). Only tags that matched in sense orientation were considered in our analysis. The RefSeq database was searched for transcripts corresponding to the regions adjacent to the alignment location of each 5′tag.

RT-PCR

Total RNA was extracted using a ToTally RNA extraction kit (Ambion, Inc., Austin, TX, USA). Total RNA (500 ng) was reverse-transcribed in a 100-μl reaction solution containing 240 U of Moloney murine leukemia virus reverse transcriptase (Promega, Madison, WI, USA), 80 U of RNase inhibitor (Promega), 4.6 mM $MgCl_2$, 6.6 mM DTT, 1 mM dNTPs, and 2 mM random hexamer (Promega), at 42 °C for 1 h. PCR was performed in a 20-μl volume containing 0.5 U of AmpliTaq DNA polymerase (Applied Biosystems), 16.6 mM $(NH_4)_2SO_4$, 67 mM Tris–HCl, 6.7 mM $MgCl_2$, 10 mM 2-mercaptoethanol, 1 mM dNTPs, and 1.5 μM sense and antisense primers, using an ABI 9600 thermal cycler (Applied Biosystems). The amplification protocol included 28–30 cycles of 95 °C for 45 s, 58 °C for 1 min, and 72 °C for 1 min. Primer sequences are shown in Supplemental Table 2. RT-PCR was performed in triplicate for each sample-primer set. Each sample was normalized relative to *polymerase (RNA) II (DNA directed) polypeptide L (POLR2L)*. *POLR2L* is a housekeeping gene that showed relatively stable gene expression in various tissues [29]. The PCR products were semi-quantitatively analyzed with ImageJ software (http://rsb.info.nih.gov/ij/).

RTD-PCR

Intron-origin transcript expression was quantified using TaqMan Universal Master Mix (Applied Biosystems). The samples were amplified using an ABI PRISM 7900HT Sequence Detection System (Applied Biosystems). Using the standard curve methods, quantitative PCR was performed in duplicate for each sample-primer set. Each sample was normalized relative to *POLR2L*. The assay IDs used were Hs00185873_m1 for *ACOX2* and Hs00360764_m1 for *POLR2L*. The specific primers and probe sequence of intronic-*ACOX2-1* were 5′-TTCATAAAGTTGTGAGCA-GAGGAAA-3′ (forward), 5′-TGCACCACTTACTGAGCATCTACTC-3′ (reverse), and 5′-ACTTCTTACCTCAGAGCTG-3′ (probe).

Analysis of pathway network

MetaCore™ software (GeneGo Inc., St. Joseph, MI) was used to investigate the molecular pathway networks of non-B, non-C HCC, HBV-HCC and HCV-HCC. All genes up-regulated more than five-fold in all HCC libraries subjected to Enrichment analysis in GO process networks by default settings ($p<0.05$).

Statistical analysis

Kruskal–Wallis tests were used to compare the expression among normal liver, non-cancerous tissues, and HCC tissues. Mann–Whitney *U* tests were also used to evaluate the statistical significance of ACOX2

gene expression levels between two groups. All statistical analyses were performed using R (http://www.r-project.org/).

Acknowledgments

The authors would like to thank Mr. Shungo Deshimaru and Ms. Keiko Harukawa for technical assistance.

Appendix A. Supplementary data

Supplementary data associated with this article can be found, in the online version, at doi:10.1016/j.ygeno.2010.01.004.

References

[1] H.B. El-Serag, K.L. Rudolph, Hepatocellular carcinoma: epidemiology and molecular carcinogenesis, Gastroenterology 132 (2007) 2557–2576.
[2] Y. Yokoi, S. Suzuki, S. Baba, K. Inaba, H. Konno, S. Nakamura, Clinicopathological features of hepatocellular carcinomas (HCCs) arising in patients without chronic viral infection or alcohol abuse: a retrospective study of patients undergoing hepatic resection, J. Gastroenterol. 40 (2005) 274–282.
[3] R.N. Aravalli, C.J. Steer, E.N. Cressman, Molecular mechanisms of hepatocellular carcinoma, Hepatology 48 (2008) 2047–2063.
[4] D.J. Duggan, M. Bittner, Y. Chen, P. Meltzer, J.M. Trent, Expression profiling using cDNA microarrays, Nat. Genet. 21 (1999) 10–14.
[5] V.E. Velculescu, L. Zhang, B. Vogelstein, K.W. Kinzler, Serial analysis of gene expression, Science 270 (1995) 484–487.
[6] T. Yamashita, S. Hashimoto, S. Kaneko, S. Nagai, N. Toyoda, T. Suzuki, K. Kobayashi, K. Matsushima, Comprehensive gene expression profile of a normal human liver, Biochem. Biophys. Res. Commun. 269 (2000) 110–116.
[7] S. Hashimoto, S. Nagai, J. Sese, T. Suzuki, A. Obata, T. Sato, N. Toyoda, H.Y. Dong, M. Kurachi, T. Nagahata, K. Shizuno, S. Morishita, K. Matsushima, Gene expression profile in human leukocytes, Blood 101 (2003) 3509–3513.
[8] H. Okabe, S. Satoh, T. Kato, O. Kitahara, R. Yanagawa, Y. Yamaoka, T. Tsunoda, Y. Furukawa, Y. Nakamura, Genome-wide analysis of gene expression in human hepatocellular carcinomas using cDNA microarray: identification of genes involved in viral carcinogenesis and tumor progression, Cancer. Res. 61 (2001) 2129–2137.
[9] Y. Shirota, S. Kaneko, M. Honda, H.F. Kawai, K. Kobayashi, Identification of differentially expressed genes in hepatocellular carcinoma with cDNA microarrays, Hepatology 33 (2001) 832–840.
[10] T. Yamashita, M. Honda, S. Kaneko, Application of serial analysis of gene expression in cancer research, Curr. Pharm. Biotechnol. 9 (2008) 375–382.
[11] Y. Suzuki, H. Taira, T. Tsunoda, J. Mizushima-Sugano, J. Sese, H. Hata, T. Ota, T. Isogai, T. Tanaka, S. Morishita, K. Okubo, Y. Sakaki, Y. Nakamura, A. Suyama, S. Sugano, Diverse transcriptional initiation revealed by fine, large-scale mapping of mRNA start sites, EMBO Rep. 2 (2001) 388–393.
[12] K. Kimura, A. Wakamatsu, Y. Suzuki, T. Ota, T. Nishikawa, R. Yamashita, J. Yamamoto, M. Sekine, K. Tsuritani, H. Wakaguri, S. Ishii, T. Sugiyama, K. Saito, Y. Isono, R. Irie, N. Kushida, T. Yoneyama, R. Otsuka, K. Kanda, T. Yokoi, H. Kondo, M. Wagatsuma, K. Murakawa, S. Ishida, T. Ishibashi, A. Takahashi-Fujii, T. Tanase, K. Nagai, H. Kikuchi, K. Nakai, T. Isogai, S. Sugano, Diversification of transcriptional modulation: large-scale identification and characterization of putative alternative promoters of human genes, Genome. Res. 16 (2006) 55–65.
[13] T. Shiraki, S. Kondo, S. Katayama, K. Waki, T. Kasukawa, H. Kawaji, R. Kodzius, A. Watahiki, M. Nakamura, T. Arakawa, S. Fukuda, D. Sasaki, A. Podhajska, M. Harbers, J. Kawai, P. Carninci, Y. Hayashizaki, Cap analysis gene expression for high-throughput analysis of transcriptional starting point and identification of promoter usage, Proc. Natl. Acad. Sci. U. S. A. 100 (2003) 15776–15781.
[14] S. Hashimoto, Y. Suzuki, Y. Kasai, K. Morohoshi, T. Yamada, J. Sese, S. Morishita, S. Sugano, K. Matsushima, 5′-end SAGE for the analysis of transcriptional start sites, Nat. Biotechnol. 22 (2004) 1146–1149.
[15] T. Yamashita, S. Kaneko, S. Hashimoto, T. Sato, S. Nagai, N. Toyoda, T. Suzuki, K. Kobayashi, K. Matsushima, Serial analysis of gene expression in chronic hepatitis C and hepatocellular carcinoma, Biochem. Biophys. Res. Commun. 282 (2001) 647–654.
[16] T. Yamashita, M. Honda, H. Takatori, R. Nishino, H. Minato, H. Takamura, T. Ohta, S. Kaneko, Activation of lipogenic pathway correlates with cell proliferation and poor prognosis in hepatocellular carcinoma, J. Hepatol. 50 (2009) 100–110.
[17] J.S. Mattick, Introns: evolution and function, Curr. Opin. Genet. Dev. 4 (1994) 823–831.
[18] J.S. Mattick, I.V. Makunin, Non-coding RNA, Hum. Mol. Genet. 15 (Spec No 1) (2006) R17–29.
[19] R. Louro, A.S. Smirnova, S. Verjovski-Almeida, Long intronic noncoding RNA transcription: expression noise or expression choice? Genomics 93 (2009) 291–298.
[20] S. Yu, S. Rao, J.K. Reddy, Peroxisome proliferator-activated receptors, fatty acid oxidation, steatohepatitis and hepatocarcinogenesis, Curr. Mol. Med. 3 (2003) 561–572.
[21] N. Kondoh, T. Wakatsuki, A. Ryo, A. Hada, T. Aihara, S. Horiuchi, N. Goseki, O. Matsubara, K. Takenaka, M. Shichita, K. Tanaka, M. Shuda, M. Yamamoto, Identification and characterization of genes associated with human hepatocellular carcinogenesis, Cancer. Res. 59 (1999) 4990–4996.
[22] Y. Kobayashi, T. Higashi, K. Nouso, H. Nakatsukasa, M. Ishizaki, T. Kaneyoshi, N. Toshikuni, K. Kariyama, E. Nakayama, T. Tsuji, Expression of MAGE, GAGE and BAGE genes in human liver diseases: utility as molecular markers for hepatocellular carcinoma, J. Hepatol. 32 (2000) 612–617.
[23] A.H. Minn, M. Kayton, D. Lorang, S.C. Hoffmann, D.M. Harlan, S.K. Libutti, A. Shalev, Insulinomas and expression of an insulin splice variant, Lancet 363 (2004) 363–367.
[24] H. Stier, H.D. Fahimi, P.P. Van Veldhoven, G.P. Mannaerts, A. Volkl, E. Baumgart, Maturation of peroxisomes in differentiating human hepatoblastoma cells (HepG2): possible involvement of the peroxisome proliferator-activated receptor alpha (PPAR alpha), Differentiation 64 (1998) 55–66.
[25] S. Zha, S. Ferdinandusse, J.L. Hicks, S. Denis, T.A. Dunn, R.J. Wanders, J. Luo, A.M. De Marzo, W.B. Isaacs, Peroxisomal branched chain fatty acid beta-oxidation pathway is upregulated in prostate cancer, Prostate 63 (2005) 316–323.
[26] K. Tokuoka, Y. Nakajima, K. Hirotsu, I. Miyahara, Y. Nishina, K. Shiga, H. Tamaoki, C. Setoyama, H. Tojo, R. Miura, Three-dimensional structure of rat-liver acyl-CoA oxidase in complex with a fatty acid: insights into substrate-recognition and reactivity toward molecular oxygen, J. Biochem. 139 (2006) 789–795.
[27] K. Meyer, Y. Jia, W.Q. Cao, P. Kashireddy, M.S. Rao, Expression of peroxisome proliferator-activated receptor alpha, and PPARalpha regulated genes in spontaneously developed hepatocellular carcinomas in fatty acyl-CoA oxidase null mice, Int. J. Oncol. 21 (2002) 1175–1180.
[28] N. Tanaka, K. Moriya, K. Kiyosawa, K. Koike, F.J. Gonzalez, T. Aoyama, PPARalpha activation is essential for HCV core protein-induced hepatic steatosis and hepatocellular carcinoma in mice, J. Clin. Invest. 118 (2008) 683–694.
[29] C. Rubie, K. Kempf, J. Hans, T. Su, B. Tilton, T. Georg, B. Brittner, B. Ludwig, M. Schilling, Housekeeping gene variability in normal and cancerous colorectal, pancreatic, esophageal, gastric and hepatic tissues, Mol. Cell. Probes. 19 (2005) 101–109.

Journal of Medical Virology 85:241–249 (2013)

Synthetic Lipophilic Antioxidant BO-653 Suppresses HCV Replication

Fumihiko Yasui,[1] Masayuki Sudoh,[2] Masaaki Arai,[3] and Michinori Kohara[1]*

[1]*Department of Microbiology and Cell Biology, Tokyo Metropolitan Institute of Medical Science, Setagaya-ku, Tokyo, Japan*
[2]*Kamakura Research Laboratories, Chugai Pharmaceutical Co., Ltd., Kanagawa, Japan*
[3]*Biologics Research Department, Advanced Medical Research Laboratories, Mitsubishi Tanabe Pharma Corporation, Osaka, Japan*

The influence of the intracellular redox state on the hepatitis C virus (HCV) life cycle is poorly understood. This study demonstrated the anti-HCV activity of 2,3-dihydro-5-hydroxy-2,2-dipentyl-4,6-di-*tert*-butylbenzofuran (BO-653), a synthetic lipophilic antioxidant, and examined whether BO-653's antioxidant activity is integral to its anti-HCV activity. The anti-HCV activity of BO-653 was investigated in HuH-7 cells bearing an HCV subgenomic replicon (FLR3-1 cells) and in HuH-7 cells infected persistently with HCV (RMT-tri cells). BO-653 inhibition of HCV replication was also compared with that of several hydrophilic and lipophilic antioxidants. BO-653 suppressed HCV replication in FLR3-1 and RMT-tri cells in a concentration-dependent manner. The lipophilic antioxidants had stronger anti-HCV activities than the hydrophilic antioxidants, and BO-653 displayed the strongest anti-HCV activity of all the antioxidants examined. Therefore, the anti-HCV activity of BO-653 was examined in chimeric mice harboring human hepatocytes infected with HCV. The combination treatment of BO-653 and polyethylene glycol-conjugated interferon-α (PEG-IFN) decreased serum HCV RNA titer more than that seen with PEG-IFN alone. These findings suggest that both the lipophilic property and the antioxidant activity of BO-653 play an important role in the inhibition of HCV replication. ***J. Med. Virol. 85:241–249, 2013.*** © 2012 Wiley Periodicals, Inc.

KEY WORDS: BO-653; antioxidant activity; chemical structure; HCV replication; chimeric mice

INTRODUCTION

Hepatitis C virus (HCV) causes persistent infection, leading to chronic liver diseases including chronic hepatitis, cirrhosis, and hepatocellular carcinoma. In 2009, the number of patients with HCV infection worldwide was estimated to be 130–170 million [Lavanchy, 2009]. Recent years have seen the development of several promising treatments for patients infected with HCV. The addition of a protease inhibitor (boceprevir or telaprevir) to polyethylene glycol-conjugated interferon-α (PEG-IFN) and ribavirin improved dramatically the sustained virological response rates in treatment-naive patients with genotype 1 infections. However, the sustained virological response rate of triple therapy with a telaprevir-based regimen in null responders treated with PEG-IFN/ribavirin is only 30% [Fontaine and Pol, 2011; Kumada et al., 2012]. There is concern that high-risk groups such as patients with the *IL28B* minor allele (re8099917 SNP; GT/GG), the elderly, or those with fibrosis will be resistant to the triple therapy [Suppiah et al., 2009; Tanaka et al., 2009]. Therefore, new therapeutic strategies are required to treat HCV infection.

Chronic HCV infection is closely associated with oxidative stress. Oxidative stress reflects an imbalance between the production of reactive oxygen species (ROS) and the activity of intracellular antioxidant systems. The cumulative evidence from experimental

Grant sponsor: Ministry of Education, Culture, Sports, Science and Technology of Japan; Grant sponsor: Program for Promotion of Fundamental Studies in Health Science of the National Institute of Biomedical Innovation of Japan; Grant sponsor: Ministry of Health, Labor and Welfare of Japan.

Conflict of interest: Dr. Sudoh is an employee of Chugai Pharmaceutical Co., Ltd. The other authors declare no potential conflicts of interest.

*Correspondence to: Michinori Kohara, Department of Microbiology and Cell Biology, Tokyo Metropolitan Institute of Medical Science, 2-1-6, Kamikitazawa, Setagaya-ku, Tokyo 156-8506, Japan. E-mail: kohara-mc@igakuken.or.jp

Accepted 9 October 2012

DOI 10.1002/jmv.23466
Published online 28 November 2012 in Wiley Online Library (wileyonlinelibrary.com).

and clinical studies demonstrates that HCV infection causes excessive ROS production and decreased activity of antioxidant enzymes [Kato et al., 2001; Levent et al., 2006]. In addition, previous studies showed that aggravation of oxidative stress in hepatocytes infected with HCV is correlated with the iron overload, while phlebotomy improves oxidative stress markers and liver pathology [Seronello et al., 2007]. Therefore, oxidative stress is a deleterious factor involved in the development of various hepatic diseases ranging from chronic hepatitis to hepatocellular carcinoma. In contrast, the influence of the intracellular redox state on HCV replication is controversial. Exogenous addition of either hydrogen peroxide or unsaturated fatty acid has been shown to induce oxidative stress and inhibit HCV replication in cell culture models [Choi et al., 2004; Huang et al., 2007]. Yano et al. [2007] reported previously that any of several nutrients (including vitamin E, a hydrophobic antioxidant) enhance HCV RNA replication. In contrast, overproduction of the antioxidant enzyme heme oxygenase-1 decreases HCV RNA replication in both full-length and subgenomic replicons [Zhu et al., 2008]. Despite these in vitro results, there have been no reports on the effect of antioxidant or pro-oxidant reagents on the life cycle of HCV in any animal models, such as chimeric mice harboring human hepatocytes infected with HCV.

BO-653 (2,3-dihydro-5-hydroxy-2,2-dipentyl-4,6-di-*tert*-butylbenzofuran), a lipophilic (hydrophobic) antioxidant, was previously a clinical candidate for potential treatment of atherosclerosis and the prevention of post-angioplasty restenosis [Cynshi et al., 1998; Meng, 2003]. This compound is an effective inhibitor of lipid peroxidation and inhibits potently oxidation of lipids such as low-density lipoprotein [Noguchi et al., 1997; Tamura et al., 2003]. The present study examined the anti-HCV activity of BO-653 both in vitro and in vivo, and sought to clarify whether the antioxidant activity of the molecule was integral to the observed anti-HCV activity.

MATERIALS AND METHODS

Chemicals

BO-653 (molecular weight [MW], 388.6) was a gift of the Chugai Pharmaceutical company (Tokyo, Japan). Probucol [4,4′-(isopropylidenedithio)bis(2,6-di-*tert*-butylphenol)] was purchased from Wako Pure Chemical Industries (Osaka, Japan). *N*-acetyl cysteine and ascorbic acid (vitamin C) were obtained from Sigma–Aldrich (St. Louis, MO). Trolox (6-hydroxy-2,5,7,8-tetramethylchroman-2-carboxylic acid) and D-α-tocopherol (vitamin E) were obtained from Calbiochem (San Diego, CA) and MP Biomedical LLC (Solon, OH), respectively.

Viruses and Cells

Patients provided written informed consent prior to blood sample collection.

HuH-7 cells harboring a HCV subgenomic replicon (FLR3-1 cells; genotype 1b, Con-1 strain) were maintained at 37°C in 5% CO_2 in Dulbecco's modified Eagle's medium GlutaMAX-I (DMEM-GlutaMax I; Invitrogen, Carlsbad, CA) supplemented with 10% fetal calf serum (FCS) and 0.5 mg/ml G418 [Inoue et al., 2007].

HuH-7 cells infected persistently with HCV (RMT-tri cells; genotype 1a) were generated in the laboratory as described below and were maintained in DMEM containing 10% FCS, nonessential amino acids, 10 mM HEPES [4-(2-hydroxyethyl)-1-piperazineethanesulfonic acid], and 0.4% glucose. Complementary DNA (cDNA) of the full-genome HCV (nucleotides 1–9,598; GenBank accession number AB520610) was prepared from the serum of a patient with acute hepatitis infected with HCV genotype 1a [Inoue et al., 2007]. The resulting serum harbored HCV at a titer of $10^{8.6}$ copies/ml, as detected by a quantitative real-time polymerase chain reaction (qRT-PCR) as described previously [Takeuchi et al., 1999]. The sequence of the final cDNA construct was determined from a consensus of more than 10 clones, and was subcloned under the control of a T7 promoter (pHCV-RMT). The construct of HCV subgenomic replicon was generated from pHCV-RMT. HCV subgenomic RNA was transcribed using T7 RNA polymerase and the MEGAscript in vitro transcription kit (Ambion, Austin, TX) according to the manufacturer's instructions. The resulting synthetic RNA of the HCV subgenomic replicon was transfected into HuH-7 cells by electroporation. Following transfection, the HCV subgenomic replicon-bearing HuH-7 cells was established. Total RNA was extracted by the acid guanidinium–phenol–chloroform method from a sample of the HCV subgenomic replicon-bearing HuH-7 cells and reverse transcribed. Sequence of the resulting cDNA has three nonsynonymous substitutions compared to that of the original HCV subgenomic replicon. Next, three nonsynonymous substitutions were inserted into the original full-length HCV sequence to enhance the replication rate in HuH-7 cells. Full-length RNA was also transcribed as described above. The resulting synthetic RNA of full-length HCV was transfected into HuH-7 cells by electroporation. Following transfection, the HCV RNA level in the transfected cells was measured on a weekly basis, revealing persistent infection at a level of $10^{6.5}$–$10^{6.8}$ copies/μg total cellular RNA over the course of 50 days. Finally, the transfected cell line was designated as RMT-tri.

Analysis of Anti-HCV Effect of BO-653 in FLR3-1 Cells

The anti-HCV activity of BO-653 in FLR3-1 cells was measured by inhibiting luciferase activity [Inoue et al., 2007]. In brief, FLR3-1 cells were seeded at 4×10^3 cells/well in 96-well white plates. After 24 hr, the culture medium was replaced with fresh medium containing various concentrations of BO-653

(12–1,000 μM). The culture medium containing 1% MeOH was used as the negative control. After 72 hr incubation, the luciferase activity of the cells was measured using the Bright-Glo luciferase assay (Promega, Madison, WI) according to the manufacturer's instructions.

Analysis of Anti-HCV Effect of BO-653 in RMT-Tri Cells

RMT-tri cells were seeded at 2.5×10^4 cells/well in 24-well plates. After 24 hr, the culture medium was replaced with fresh medium containing various concentrations of BO-653 (12–1,000 μM). The culture medium containing 1% MeOH was used as the negative control. After 72 hr incubation, the cell monolayer was harvested by adding 400 μl of 5 M guanidine-isocyanate solution containing 5.6 μl of 2-mercaptoethanol. The total RNA was extracted as above; HCV RNA was quantified by qRT-PCR.

Comparison of Anti-HCV Activity of Lipophilic and Hydrophilic Antioxidants

The anti-HCV activity of various antioxidants, including hydrophilic and lipophilic compounds, was compared in FLR3-1 cells. BO-653, α-tocopherol, and probucol were used as lipophilic antioxidants; *N*-acetyl cysteine, ascorbic acid, and trolox were used as hydrophilic antioxidants. The anti-HCV activities of these compounds were determined by luciferase assays as described above.

Cytotoxicity Testing

Simultaneously with the luciferase assays, the cell viability was measured by using a WST-8 cell counting kit (Dojindo, Kumamoto, Japan) according to the manufacturer's instructions.

Western Blot Analysis

FLR3-1 cells were treated with BO-653 as described above. After 96 hr, the cells were lysed with lysis buffer (protease inhibitor cocktail [Complete, Roche Diagnostics, IN] formulated according to the manufacturer's instructions in 10 mM Tris [pH 7.4], 150 mM NaCl, 1% sodium dodecyl sulfate (SDS), 0.5% Nonidet P-40). The cell lysates were resolved by SDS–polyacrylamide gel electrophoresis and transferred to polyvinylidene fluoride membranes. After incubation with a blocking buffer consisting of 5% skim milk in Tris-buffered saline containing 0.1% Tween 20 [TBS-T], the membranes were incubated with rabbit polyclonal anti-NS3 antibody (R212 clone) and goat anti-rabbit IgG horseradish peroxidase (HRP)-conjugated IgG (GE Healthcare, Little Chalfont, Buckinghamshire, UK) as the primary and secondary antibodies, respectively. Labeling was visualized using the Immobilon Western system (Millipore, Billerica, MA). To provide a loading control, β-actin was detected using mouse anti-β-actin monoclonal antibody (Sigma-Aldrich) and sheep anti-mouse IgG HRP-conjugated IgG (GE Healthcare) as the primary and secondary antibodies, respectively.

Immunofluorescent Staining

FLR3-1 cells treated with 111 μM BO-653 for 96 hr were probed with the primary antibody (anti-NS3) after blocking with TNB blocking buffer (PerkinElmer, Waltham, MA). An anti-rabbit IgG Alexa-Fluor 488 conjugate (Invitrogen, Grand Island, NY) was then applied as the secondary antibody.

Measurement of Antioxidant Activity of BO-653, α-Tocopherol, and Probucol in Lipid Peroxidation

Oxidation of methyl linoleate (10 mM) was carried out at 37°C under air in acetonitrile solution by adding 0.2 mM AMVN (2,2′-azobis-2,4-dimethylvaleronitrile) as a radical initiator in the presence of various concentrations of BO-653, α-tocopherol, and probucol. These antioxidants were added at concentrations of 0.2–20 μM to the reaction mixture; after 60 min incubation at 37°C, the reactions were stopped by chilling on ice.

The levels of lipid peroxidation were determined by the ferrous oxidation-xylenol orange (FOX) method [Nourooz-Zadeh et al., 1994]. In brief, completed methyl linoleate oxidation reactions were diluted 10-fold with MeOH containing 4.4 mM 2,6-di-*tert*-butyl-4-methylphenol (BHT). Each diluted solution (1.8 ml) was mixed with 0.1 ml of 2 mM xylenol orange solution (in 250 mM H_2SO_4) and 0.1 ml of 5 mM ferrous chloride solution (in 250 mM H_2SO_4). The mixture was incubated at room temperature for 60 min, at which point the absorbance at 570 nm was measured using a UV/visible light spectrophotometer. Cumene hydroperoxide was used to generate a standard curve for lipid hydroperoxidation.

Pharmacokinetics of BO-653 in uPA/SCID Mice Harboring Human Hepatocytes

Chimeric uPA/SCID mice harboring human hepatocytes were purchased from PhoenixBio (Hiroshima, Japan). All animal experiments were approved by the Ethics Committee of Tokyo Metropolitan Institute of Medical Science and were performed in accordance with the guidelines of the Animal Experimental Committee of Tokyo Metropolitan Institute of Medical Science. Two chimeric mice were administered BO-653 (at 800 or 2,000 mg/kg in 3% gum arabic solution) by single oral gavage. At 24 hr after administration, blood was collected and the plasma concentration of BO-653 was measured by high-performance liquid chromatography (HPLC). Aliquots of plasma (100 μl) were mixed with 50 μl MeOH containing 10 mM ascorbic acid and 100 μl acetonitrile containing 30 μg/ml MeO-BO-653 as the internal control. The mixtures were centrifuged at 9,100*g* for 5 min, and the resulting supernatants of 30 μl each were separated using

an octadecyl column (Capcell Pak C18 UG120, 3 μm, 4.6 mm × 50 mm; Shiseido, Tokyo, Japan) at 30°C, a detection wavelength of 300 nm, and an eluent (acetonitrile) flow rate of 1.0 ml/min.

Treatment of HCV-Infected Chimeric Mice With BO-653 and/or PEG-IFN

Chimeric mice also were used as an in vivo model of persistent HCV infection, as described previously [Inoue et al., 2007]. uPA/SCID mice were engrafted with human hepatocytes; 6 weeks later, the chimeric mice were infected by intravenous (IV) injection with patient serum containing 10^6 copies of HCV genotype 1b (HCR6; GenBank accession no. AY045702). By 4 weeks after infection, the HCV RNA levels reached a plateau of 10^6–10^7 copies/ml of mouse serum. To determine anti-HCV activity of BO-653 in the early phase of the treatment, the chimeric mice (n = 2–5 per group) infected with HCV were given once-daily oral gavage with 2,000 mg/kg BO-653 in 3% gum arabic, and/or twice weekly subcutaneous injection with 30 μg/kg PEG-IFNα-2a (Chugai Pharmaceutical) as shown in Table I. Body weights were monitored daily, and blood for serum was collected prior to the start of treatment (Day-1) and once weekly thereafter (Days 8 and 14). Following the terminal bleed, animals were sacrificed and liver specimens were collected.

Quantitation of HCV RNA by qRT-PCR

After completion of the treatment, total RNA was purified from the serum and liver specimens by the acid guanidinium-phenol-chloroform method and qRT-PCR was used to quantify HCV RNA from the RNA samples corresponding to 1 μl serum and about 5 mm^3 of liver.

Quantitation of Serum Human Albumin

The human albumin concentration in the blood of chimeric mice was measured in 2-μl serum samples by using an Alb-II kit (Eiken Chemical, Tokyo, Japan) according to the manufacturer's instructions.

Statistical Analysis

Data are presented as mean ± standard deviations (SDs). Statistical analysis was performed by using either Student's *t*-test or ANOVA, followed by Tukey's test or Dunnett's test. A value of $P < 0.05$ was considered statistically significant.

RESULTS

Inhibitory Effect of BO-653 on HCV Replication In Vitro

The anti-HCV activity of BO-653 (Fig. 1A) was investigated in cells harboring HCV subgenomic replicons (FLR3-1 cells). BO-653 suppressed the replication of HCV subgenomic replicons in a concentration-dependent manner (Fig. 1B). The half-maximal inhibitory concentration (IC_{50}) of BO-653 in FLR3-1 cells was 36.0 μM. In contrast, no cytotoxicity was observed with up to 1,000 μM of BO-653 in FLR3-1 cells (Fig. 1B). Western blotting and immunofluorescent staining of FLR3-1 cells demonstrated that the level of HCV NS3 protein, but not that of β-actin, was reduced as the concentrations of BO-653 increased (Fig. 1C and D). A similar trend was seen in RMT-tri cells for the replication of full-genome HCV genotype 1a (Fig. 1E).

Comparison of Anti-HCV Activity of Lipophilic Antioxidants

The antioxidant activity of BO-653 has been compared previously with that of probucol and α-tocopherol [Cynshi et al., 1998]. Therefore, the anti-HCV activity of these three lipophilic antioxidants was compared in FLR3-1 cells. At a concentration >37 μM, BO-653 exhibited stronger inhibitory effects against HCV replication than did the two other compounds (Fig. 2A). In addition, the antioxidant activity of these compounds was determined by an in vitro lipid peroxidation system. BO-653 had the strongest antioxidant activity against lipid peroxidation in this in vitro assay (Fig. 2C).

Comparison of Anti-HCV Activity of Hydrophilic and Lipophilic Antioxidants

The anti-HCV activities of some representative antioxidants were investigated further (Fig. 3A). As noted above, lipophilic antioxidants exhibited anti-HCV activity in cell culture; however, hydrophilic antioxidants (*N*-acetyl cysteine, ascorbic acid, and trolox) did not inhibit the replication of HCV subgenomic replicons at comparable concentrations. None of the

TABLE I. Schedule of Blood Collection and Drug Administration for Chimeric Mice Infected With HCV

	Day															
	−1	0	1	2	3	4	5	6	7	8	9	10	11	12	13	14
Collection of blood	B									B						B
BO-653		BO	BO	BO	BO	BO	BO	BO	BO	BO	BO	BO	BO	BO	BO	
PEG-IFN		I			I				I			I				
BO-653 + PEG-IFN		BO/I	BO	BO	BO/I	BO	BO	BO	BO/I	BO	BO	BO/I	BO	BO	BO	

B, sampling of blood; BO, orally administrated BO-653 (2,000 mg/kg); I, subcutaneous injection of PEG-IFN (30 μg/kg).

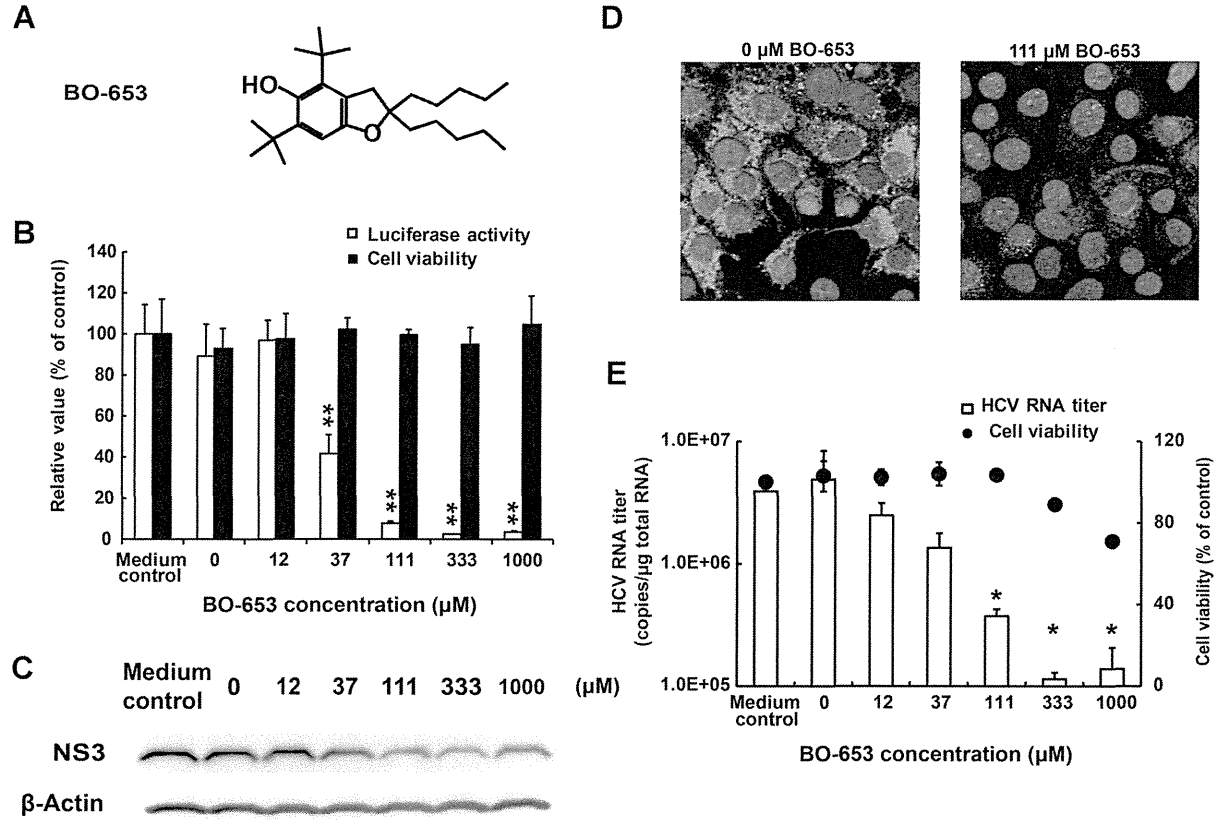

Fig. 1. In vitro anti-HCV activity of BO-653. **A**: The chemical structure of BO-653. **B**: The inhibitory effect of BO-653 on the replication of HCV subgenomic replicons in FLR3-1 cells. HCV replication (white bars) and cell viability (black bars) were determined after 72 hr of treatment; $^{**}P < 0.01$, compared with the medium control. **C**: Effect of BO-653 on the levels of HCV NS3 protein and β-actin (Western blotting). **D**: Immunofluorescent staining of HCV NS3 protein (green) in FLR3-1 cells in the absence or presence (111 μM) of BO-653; nuclei were stained with 4′,6-diamidino-2-phenylindole (blue). **E**: Effect of BO-653 on the HCV RNA titer and cell viability of HuH-7 cells infected with HCV genotype 1a (RMT-tri) after 72 hr of treatment; $^{*}P < 0.05$, compared with the medium control. Statistical analyses were performed by using ANOVA with post-hoc Dunnett's (n = 3 replicates).

compounds had any cytotoxicity at the concentrations tested (Fig. 3B).

Anti-HCV Activity of BO-653 and PEG-IFN in Chimeric Mice Infected With HCV

As demonstrated above using an in vitro assay with FLR3-1 cells, lipophilic antioxidants, including BO-653, exhibited strong anti-HCV activity. The anti-HCV activity of BO-653 was assessed further in vivo by using the compound to treat humanized chimeric mice infected with HCV. First, to measure the pharmacokinetics of BO-653, two chimeric mice were administered orally BO-653 at 800 or 2,000 mg/kg. Twenty-four hours after administration, the mice had mean BO-653 plasma concentrations of 25.0 and 83.1 μM, respectively (Table II). Thus, the BO-653 plasma concentration at the higher dose level exceeded the IC_{50} of BO-653 (36.0 μM) demonstrated previously by the in vitro assay (Fig. 1B), suggesting that oral administration of 2,000 mg/kg BO-653 might be relevant therapeutically for chimeric mice infected with HCV. These mice were infected persistently with HCV genotype 1b by injection with the serum of a HCV-infected patient (see Materials and Methods Section). To determine the anti-HCV activity of BO-653 in early phase of treatment, BO-653 (oral) and/or PEG-IFN (subcutaneous) were then administered over a period of 14 days, according to the schedule shown in Table I, and serum and liver specimens were collected. No adverse effect of the treatment, such as loss of body weight or decreased human albumin secretion, was observed in any of the study groups (Fig. 4A and B). In the mice treated with PEG-IFN, which received a dose 20-fold higher dose than that used in the clinic, the serum HCV RNA titers fell approximately 30-fold and 50-fold in weeks 1 and 2, respectively. Treatment with BO-653 alone at 2,000 mg/kg orally once daily did not reduce the HCV RNA serum titers. However, the combination of BO-653 and PEG-IFN was effective, with the combination demonstrating 200-fold decrease in serum

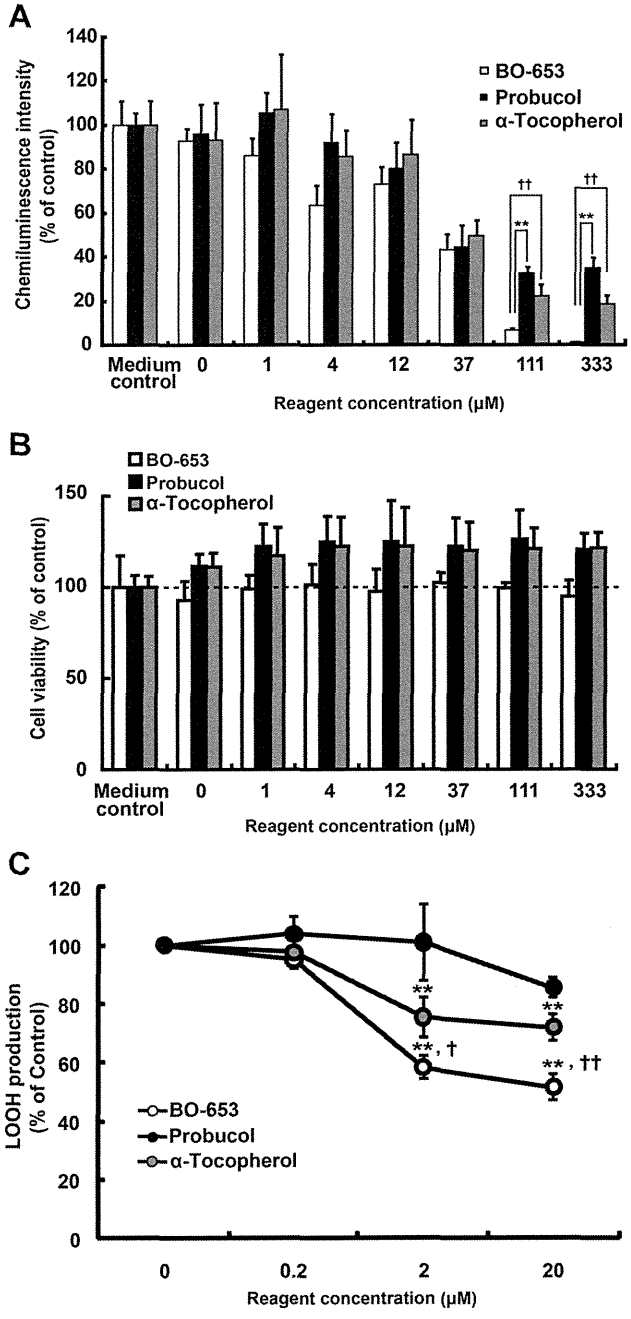

Fig. 2. Comparison of the in vitro anti-HCV activities of lipophilic antioxidants. **A**: The anti-HCV activity and (**B**) cytotoxicity of BO-653, α-tocopherol, and probucol were measured in FLR3-1 cells after 72 hr exposure to the compounds; $^{**}P < 0.01$, compared with probucol at the same concentration, $^{\dagger\dagger}P < 0.01$, compared with α-tocopherol at the same concentration. **C**: Antioxidant activity of BO-653, α-tocopherol, and probucol in the peroxidation of methyl linoleate with AMVN (FOX method); $^{**}P < 0.01$, compared with probucol at the same concentration, and $^{\dagger}P < 0.05$ and $^{\dagger\dagger}P < 0.01$, compared with α-tocopherol at the same concentration. Statistical analyses were performed using ANOVA with post-hoc Tukey's.

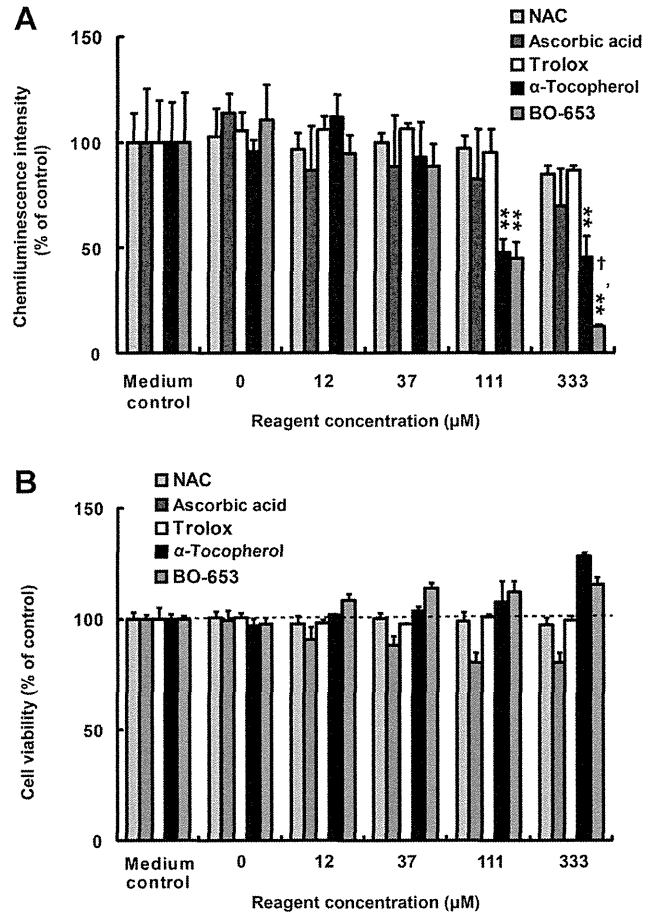

Fig. 3. Comparison of the anti-HCV activity of lipophilic and hydrophilic antioxidants. **A**: The anti-HCV activity and (**B**) cytotoxicity of BO-653 and α-tocopherol (lipophilic antioxidants) and *N*-acetyl cysteine (NAC), ascorbic acid, and trolox (hydrophilic antioxidants) in FLR3-1 cells after 72 hr of exposure to the compounds. $^{**}P < 0.01$, compared with the hydrophilic antioxidants at the same concentration, and $^{\dagger}P < 0.05$, compared with α-tocopherol at the same concentration. Statistical analyses were performed using ANOVA with post-hoc Tukey's.

HCV titer at 2 weeks; the effect was statistically significant compared to treatment with PEG-IFN alone (Fig. 4C). In the liver samples, a decrease in the titer of HCV RNA to 7–34% of the value in untreated mice was also observed in the mice given the combination therapy (Fig. 4D).

DISCUSSION

Several lines of evidence indicate that chronic HCV infection is associated with persistently elevated levels of ROS, resulting in oxidative stress and thus contributing to the development of hepatic dam-

TABLE II. Concentration of BO-653 in Plasma

Dose	Mouse ID	Concentration of BO-653 in plasma (μM)	Mean concentration (μM)
800 mg/kg	1	30.2	25.0
	2	19.8	
2,000 mg/kg	1	100.9	83.1
	2	65.2	

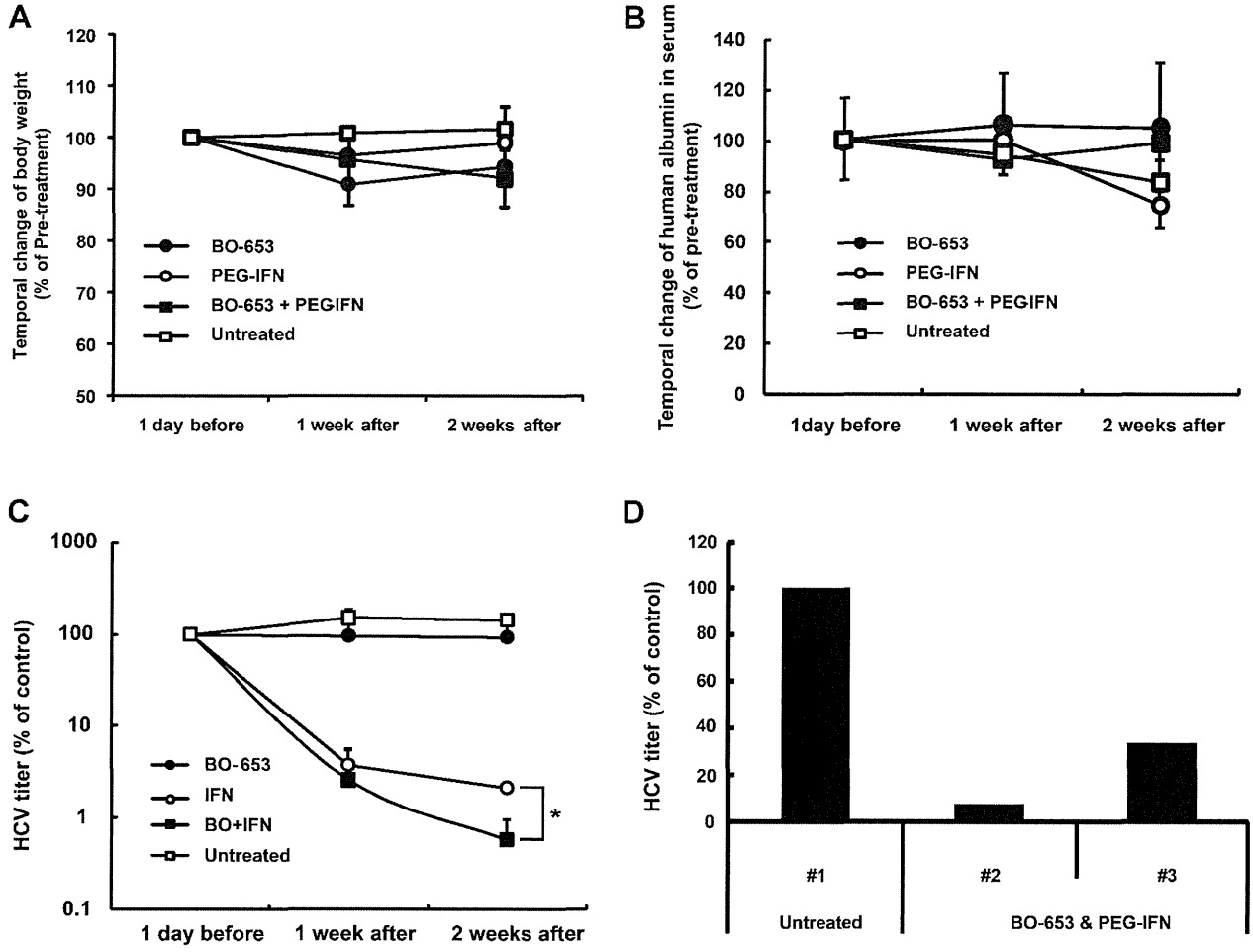

Fig. 4. Anti-HCV effect of BO-653 in chimeric mice infected with HCV. Temporal changes in the (**A**) body weight, (**B**) human albumin concentration in the serum, and (**C**) HCV RNA titer in the serum of chimeric mice infected with HCV after the indicated treatments. All groups included 3–5 mice, except for the untreated group (n = 2). The mice received once-daily oral gavage with 2,000 mg/kg BO-653 and/or twice-weekly subcutaneous injection with 30 μg/kg PEG-IFNα-2a (see Table I). The HCV RNA titers were normalized to the pre-treatment (Day-1) titer in the respective mouse. $^{*}P < 0.05$, PEG-IFN and BO-653 combination treatment (n = 5) was compared with PEG-IFN monotherapy (n = 3) of the same duration. Statistical analyses were performed using Student's *t*-test. **D**: The HCV RNA titer in the liver of chimeric mice treated with or without PEG-IFN and BO-653 combination treatment (untreated group, n = 1; combination treatment group, n = 2).

age [Shimoda et al., 1994; Bureau et al., 2001; Gong et al., 2001; Waris et al., 2005; Levent et al., 2006]. On the other hand, the influence of the intracellular redox state on HCV replication is controversial. A previous study demonstrated inhibition of HCV subgenomic replicon replication by lipid peroxidation and restoration of the replication by treatment with vitamin E [Huang et al., 2007]. A similar result was reported by Choi et al. [2004], who showed inhibition of HCV replication by exogenous hydrogen peroxide treatment. These results indicate that elevated levels of ROS, higher than those induced by natural HCV infection, can lead to inhibition of HCV replication. Yano et al. [2007] reported that several antioxidants, including vitamin E and β-carotene, enhance the replication of HCV genome-length replicons at relatively low concentrations (<10 μM). In contrast, the antioxidant pyrrolidine dithiocarbamate can suppress HCV replication via the inhibition of STAT-3 activation [Waris et al., 2005]. Notably, these studies have been performed primarily in in vitro systems, using either subgenomic replicon-containing cells, full-genome replicon-containing cells, or cells persistently infected with HCV. Therefore, clarification of the effect of antioxidants on HCV replication will require further work, including the use of in vivo models.

BO-653 (2,3-dihydro-5-hydroxy-2,2-dipentyl-4,6-di-*tert*-butylbenzofuran), a lipophilic (hydrophobic) antioxidant, was investigated clinically for potential treatment of atherosclerosis and prevention of post-angioplasty restenosis [Cynshi et al., 1998; Meng, 2003]. Starting in November 2001, a phase II trial tested BO-653